Journal of Computational Physics 231 (2012) 7695–7714

Contents lists available at SciVerse ScienceDirect

Journal of Computational Physics

journal homepage: www.elsevier.com/locate/jcp

Sparse spectral-tau method for the three-dimensional helically reduced wave equation on two-center domains

Stephen R. Lau [a,*], Richard H. Price [b]

[a] Department of Mathematics and Statistics, University of New Mexico, Albuquerque, NM 87131, United States
[b] Center for Gravitational Wave Astronomy and Center for Advanced Radio Astronomy, Department of Physics and Astronomy, University of Texas at Brownsville, Brownsville, TX 78520, United States

ARTICLE INFO

Article history:
Received 14 June 2011
Received in revised form 1 July 2012
Accepted 3 July 2012
Available online 14 July 2012

Keywords:
Spectral methods
Gravitational waves
Wave equation
Mixed-type problems
Preconditioning
Helical symmetry

ABSTRACT

We describe a multidomain spectral-tau method for solving the three-dimensional helically reduced wave equation on the type of two-center domain that arises when modeling compact binary objects in astrophysical applications. A global two-center domain may arise as the union of Cartesian blocks, cylindrical shells, and inner and outer spherical shells. For each such subdomain, our key objective is to realize certain (differential and multiplication) physical-space operators as matrices acting on the corresponding set of modal coefficients. We then achieve sparse realizations through the integration "preconditioning" of Coutsias, Hagstrom, Hesthaven, and Torres. Since ours is the first three-dimensional multidomain implementation of the technique, we focus on the issue of convergence for the global solver, here the alternating Schwarz method accelerated by GMRES. Our methods may prove relevant for numerical solution of other mixed-type or elliptic problems, and in particular for the generation of initial data in general relativity.

1. Introduction and preliminaries

1.1. Introduction

This paper describes spectral methods designed with a specific application in mind: numerical solution of a mixed-type problem arising in gravitational physics. In reviewing an ongoing program to construct helically symmetric solutions to the Einstein equations, this introduction recalls the origins of this problem below. However, this paper also serves another purpose; it demonstrates that spectral-tau *integration preconditioning*[1] yields accurate numerical solutions to the helically reduced wave equation (HRWE), a mixed-type, variable coefficient, linear partial differential equation (PDE) problem, here posed on a nontrivial three-dimensional (3D) domain. Ref. [1] offered spectral-tau integration preconditioning as a general-purpose strategy for spectral approximation of differential equations, and that reference provides the most thorough description and analysis of the technique; related techniques were explored in [2] (integration postconditioning) and [3] (nodal integration preconditioning), with applications described in, for example, Refs. [4,5]. Heretofore, spectral-tau integration preconditioning has primarily been studied either in the ODE context or for PDE problems posed on basic two-dimensional (2D) domains (rectangles, annuli, and disks); however, as a warmup to the 3D problem addressed here, we have earlier studied it in a multidomain context for the 2D HRWE [6]. While the 3D HRWE is of interest on its own, here it serves to demonstrate the general challenges

* Corresponding author.
E-mail addresses: lau@math.unm.edu (S.R. Lau), rprice@phys.utb.edu (R.H. Price).

[1] We use this term to refer to a specific technique reviewed below; however, insofar as our work is concerned the word *preconditioning* might be a misnomer. In any case, the technique does achieve *sparsification*, and this is the aspect of the technique we focus on here.

0021-9991/$ - see front matter © 2012 Elsevier Inc. All rights reserved.
http://dx.doi.org/10.1016/j.jcp.2012.07.006

and conditioning issues encountered in applying spectral-tau integration preconditioning to a 3D multidomain problem. We now describe the physical problem motivating our work.

The advent of gravitational wave detection has driven theoretical studies of gravitational wave sources. A source that is possibly interesting for ground-based detectors, and perhaps the most exciting source for space-based detectors, is the inspiral of two comparable mass black holes and their merger to form a single black hole. The early stage of inspiral is modeled with reasonable accuracy by perturbations of the Newtonian analysis, and the post-merger stage can be analyzed with black hole perturbation theory. The most difficult stage to analyze is the intermediate stage, when a few orbits remain. This epoch of inspiral is too late for a modified Newtonian approach, but too early for black hole perturbation theory. Yet this is the epoch in which a large part of the gravitational wave energy is generated.

The importance of, and difficulty in, analyzing this epoch was the original motivation for an innovative approximation, the periodic standing wave (PSW) method. This approach uses the fully nonlinear field interactions, but models the binary compact objects as forever on circular orbits of constant radius. Therefore, both the compact source motions and the fields exhibit helical symmetry. Not only does this symmetry reduce the number of independent variables, it also changes the nature of the governing PDEs, turning the problem from the hyperbolic evolution of initial data to one of mixed-type that is elliptic near a rotation axis and hyperbolic well outside the axis and beyond the orbits in the wave zone of the system. More details of this astrophysical background are given in [6]. Here we only point out that recent supercomputer evolutions of initial black hole binary data have been run stably for many orbits in the intermediate epoch. See, for example, Refs. [7–23] (not an exhaustive list), and [24] for a recent review. Even the inspiral of binaries with large mass ratios [21,22] or high spins [23], both particularly challenging cases, can now be computed. To be sure, recent successes with purely hyperbolic numerical evolutions have undercut the original motivation for the PSW approximation. Nevertheless, there remains a niche for the PSW approximation for the following reasons. First, it should provide a test bench for understanding nonlinear gravitational radiation reaction as a local process. Second, a helically symmetric solution of the Einstein equations would be, of its own accord, of bewitching interest.

The numerical computation of PSW fields has, in fact, already been carried out, using a single grid and a unique method devised especially for the problem by one of us (RHP) and coworkers. These computations were done in a series of steps [25–29] moving from linearized scalar fields up to and including the nonlinear tensor fields of general relativistic gravity. However, the method used proved too limited in accuracy to be useful. Furthermore, despite the attractive simplicity of the computational method, its implementation for general relativistic tensor fields proved challenging. The astrophysical PSW problem, therefore, can be viewed as yet unsolved. The spectral methods described here are designed to solve this astrophysical problem to high accuracy. In any case, as mentioned above, our work is relevant as a successful use of spectral-tau integration preconditioning for the solution of PDEs (even of mixed-type) on nontrivial 3D domains. From this standpoint, the astrophysical problem simply provides a convenient application, with a particularly interesting feature. In the astrophysical problem, the region in which the PDEs are hyperbolic (the distant wave zone) is a region in which the PDEs have only very small nonlinearities. The strong linearities, near the source objects, are confined to a region in which the PDEs are elliptic. While we do not consider nonlinearities in this paper, the methods we introduce for our linear model problem deliver sufficient accuracy that nonlinearities can almost surely be included.

Multidomain spectral methods for the binary inspiral of compact relativistic objects are not new. In pioneering work, nodal (i.e. collocation) methods were used by Pfeiffer et al. [30,31] for the elliptical problem of constructing binary black hole initial data, and are now being used by the Caltech-Cornell-CITA collaboration (see, for example, [20]) in the hyperbolic evolution problem. This work, now highly developed, relies on SpEC (the Spectral Einstein Code [32]), a large C++ project chiefly developed by Pfeiffer, Kidder, and Scheel, but also involving many other researchers and developers. In fact, the domain decomposition of Refs. [30,31] has motivated our own choice. Nevertheless, to date the 3D problem we consider here has not been numerically solved via spectral methods.

Our previous study [6] applied a modal multidomain spectral-tau method to a model nonlinear problem of two strong field sources in binary motion with only two spatial dimensions. That study also relied on integration preconditioning, although the relevant linear systems were inverted by direct rather than iterative methods (which was possible since the 2D problem was less memory intensive). Our 2D study, a proof of concept, showed that high accuracy could be achieved with relatively modest memory and run-time requirements. Here we generalize our 2D method to 3D, that is to three spatial dimensions and one time dimension, reduced to a problem with three independent variables by the imposition of helical symmetry. Due to the larger set of modes needed for the 3D problem, iterative solution of the relevant linear system is now necessary. We use the generalized minimum residual method (GMRES) [33,34]. Since the amount of work and storage per iteration increases with the iteration count [33,34], preconditioning is a crucial issue (and here we mean further, one might even say *genuine*, preconditioning on top of the "integration preconditioning"). Through a multilevel preconditioning scheme, we will achieve near round-off accuracy for large truncations ($\simeq$ 600,000 unknowns) with modest iteration counts. Moreover, as we achieve a sparse formulation of the relevant linear system, each iteration is also fast.

1.2. Specification of the problem

Before writing down our mixed-type PDE problem, we describe the two-center (hereafter 2-center) domain $\mathcal{D}$ on which the problem is posed, first recalling the coordinate conventions of [26]. Let $\{x, y, z\}$ represent the inertial Cartesian system

related to the spherical-polar system $\{r,\theta,\phi\}$ in the usual physicist's convention (θ and ϕ are respectively the polar and azimuthal angles). We then introduce a "comoving" Cartesian system

$$\widetilde{z} = r\cos\theta, \quad \widetilde{x} = r\sin\theta\cos(\phi-\Omega t), \quad \widetilde{y} = r\sin\theta\sin(\phi-\Omega t), \tag{1}$$

where $\Omega < 1$ is a fixed rotation rate. Note that the $\widetilde{z}$ and z-axes coincide, and both are the azimuthal axis. Via a simple permutation, we then define a new comoving system

$$\widetilde{X} = \widetilde{y}, \quad \widetilde{Y} = \widetilde{z}, \quad \widetilde{Z} = \widetilde{x} \tag{2}$$

for which the $\widetilde{Z}$-axis is not the azimuthal axis. If we imagine two compact objects with "centers" located at $\xi_1(t) = a_1\cos(\Omega t)\mathbf{e}_x + a_1\sin(\Omega t)\mathbf{e}_y$ and $\xi_2(t) = -a_2\cos(\Omega t)\mathbf{e}_x - a_2\sin(\Omega t)\mathbf{e}_y$ in the inertial $\{x,y,z\}$ system, then the $\widetilde{Z}$-axis connects these compact objects. That is, $\xi_1 = a_1\mathbf{e}_{\widetilde{Z}}$ and $\xi_2 = -a_2\mathbf{e}_{\widetilde{Z}}$. We introduce the coordinates $\{\widetilde{r},\widetilde{\theta},\widetilde{\varphi}\}$ as spherical coordinates relative to the comoving $\{\widetilde{x},\widetilde{y},\widetilde{z}\}$ system. We will exclusively work with the *comoving* systems (or simple translations or polar versions thereof), but we will often suppress tildes when doing so will not cause confusion. We will, for example, use $\{r,\theta,\varphi\}$, hereafter, to mean $\{\widetilde{r},\widetilde{\theta},\widetilde{\varphi}\}$; these coordinates should not be confused with $\{r,\theta,\phi\}$ of Eq. (1).

Relative to the system $\{\widetilde{X},\widetilde{Y},\widetilde{Z}\}$, the 2-center domain $\mathcal{D}$ that we have used is depicted in Fig. 1. Topologically, the domain $\mathcal{D}$ is a large solid 3D ball with two excised regions (each a smaller solid 3D ball). The global domain $\mathcal{D}$ has been broken into 11 subdomains, each sufficiently simple to allow for spectral expansions in terms of classical basis functions. A large outer shell (labeled O for "out") is not shown in Fig. 1, but the remaining 10 subdomains which comprise the "inner region" are shown. The inner region is comprised of two "inner shells" (spherical shells labeled J and H), three "blocks" (rectangular subdomains labeled B, C, and D), and five "cylinders" (cylindrical shells labeled $1, 2, 3, 4$, and 5).

The HRWE problem we consider is as follows:

$$L\psi = g \text{ on } \mathcal{D}, \quad \psi = h^- \text{ on } \partial H^- \cup \partial J^-, \quad \left(\frac{\partial}{\partial r} - \Omega\frac{\partial}{\partial\varphi} + \frac{1}{r}\right)\psi = h^+ \text{ on } \partial O^+, \tag{3}$$

where the defining operator is

$$L = \frac{\partial^2}{\partial\widetilde{x}^2} + \frac{\partial^2}{\partial\widetilde{y}^2} + \frac{\partial^2}{\partial\widetilde{x}^2} - \Omega^2\left(\widetilde{x}\frac{\partial}{\partial\widetilde{y}} - \widetilde{y}\frac{\partial}{\partial\widetilde{x}}\right)^2 = \frac{\partial^2}{\partial\widetilde{X}^2} + \frac{\partial^2}{\partial\widetilde{Y}^2} + \frac{\partial^2}{\partial\widetilde{Z}^2} - \Omega^2\left(\widetilde{Z}\frac{\partial}{\partial\widetilde{X}} - \widetilde{X}\frac{\partial}{\partial\widetilde{Z}}\right)^2. \tag{4}$$

Here the constant Ω is the rotation rate, and g is a prescribed source. As described in, for example, [6] this problem arises via a helical reduction of the inhomogeneous 3+1 wave equation (see also the Appendix). Notice that the problem includes Dirichlet conditions set on the inner boundaries of the spherical shells J and H. The boundary condition set on the outer boundary of the spherical shell O is of radiative type, and is here expressed in terms of the polar coordinates $\{r,\theta,\varphi\}$ relative to $\{\widetilde{x},\widetilde{y},\widetilde{z}\}$. Although this radiation condition is described precisely below, it may here be thought of as an inhomogeneous Sommerfeld condition. (The inhomogeneity h^+ in (3) is a nonlocal expression.) This paper will consider only the variable-coefficient *linear* problem (3). For numerical tests, g is taken as zero on $\mathcal{D}$, but with distributional support, point sources, located at the centers, ξ_1 and ξ_2, of J and H. For this choice of g, an exact solution is described in the Appendix. While we only consider the linear scalar problem (3), the helical reduction of the Einstein equations described in [27,28] involves a tensorial field resolved into ten coupled "helical scalars" $\psi^{(\alpha\beta)}$ each of which obeys a copy $L\psi^{(\alpha\beta)} = g^{(\alpha\beta)}$ of the above equation. However, for this formulation $g^{(\alpha\beta)}$ is now not an external source, but rather is a nonlinear coupling function of the helical scalars which

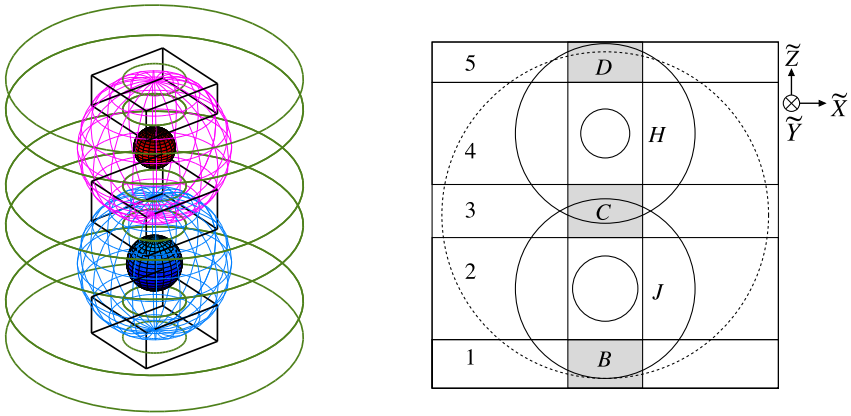

(a) 3d view of domain decomposition. (b) Cross-sectional view.

Fig. 1. Domain decomposition. The whole inner configuration of 10 subdomains is enclosed within an outer spherical shell which is not shown, save for its inner boundary in (b). Our total configuration is therefore comprised of 11 subdomains.

does include second-order derivative terms (albeit of quadratic smallness). The linear problem solved here is therefore the first step towards considering the helically reduced Einstein equations.

1.3. Overview of 3D spectral-tau integration "preconditioning"

Mostly focusing on the 3D HWRE in three Cartesian variables on a rectangular block, this subsection gives an overview of integration preconditioning for spectral-tau methods, focusing on the Kronecker product representations necessary for 3D. Our overview aims to provide the reader with enough context to follow the heavy details encountered later when applying the technique on 3D spherical and cylindrical shells. Our earlier paper [6] gave a fuller account of the same issues for 2D, many of which change little in going to 3D.

The following overview makes use of matrices D^k and $B^m_{[n]}$. These respectively represent kth order differentiation and mth order integration with respect to a basis of Chebyshev polynomials. As explained later, the subscript $[n]$ indicates that the first n rows of a matrix are empty. The following key properties are exploited later: (i) D^k is dense upper triangular, (ii) $B^m_{[n]}$ is sparse and banded with upper and lower bandwidth m, and (iii) $B^n_{[n]}D^k = B^{n-k}_{[n]}$ for $n \geqslant k$. Here $B^0_{[n]} \equiv I_{[n]}$ is the identity matrix, except that each entry in its first n rows is a 0. For the standard interval $[-1,1]$ our earlier paper [6] gave expressions for $D \equiv D^1, D^2$, $B_{[1]} \equiv B^1_{[1]}$, and $B^2_{[2]}$ (simple rescalings are necessary for a general interval); our treatment of the 3D HRWE (a second order equation) relies on these matrices.

1.3.1. Direct product representations

A function on any of our 3D subdomains is encoded by the modal coefficients in its spectral expansion, and this set of modal coefficients is often here viewed as a direct (Kronecker) product. For example, we take a rectangular block delineated by the above comoving coordinates $\{\widetilde{X},\widetilde{Y},\widetilde{Z}\}$, but for the rest of this overview we suppress the tildes on these coordinates. Suppose a function $\psi(X,Y,Z)$ on the block is approximated by the finite series

$$\mathcal{P}_{N_X,N_Y,N_Z}\psi(X,Y,Z) = \sum_{n=0}^{N_X}\sum_{m=0}^{N_Y}\sum_{p=0}^{N_Z}\widetilde{\psi}_{nmp}T_n(\xi(X))T_m(\eta(Y))T_p(\chi(Z)), \tag{5}$$

where $(\xi(X),\eta(Y),\chi(Z))$ maps our block to $[-1,1]^3$ and the $T_n(\xi)$ are Chebyshev polynomials of the first kind. Then $\psi(X,Y,Z)$ is represented (either exactly or approximately) by a three-index set $\{\widetilde{\psi}_{nmp} : 0 \leqslant n \leqslant N_X,\ 0 \leqslant m \leqslant N_Y,\ 0 \leqslant p \leqslant N_Z\}$ of modal coefficients. We view this set as a vector $\widetilde{\boldsymbol{\psi}}$, with components $\widetilde{\boldsymbol{\psi}}(\alpha)$ fixed by the direct product representation

$$\widetilde{\boldsymbol{\psi}}(n(N_Y+1)(N_Z+1)+m(N_Z+1)+p) = \widetilde{\psi}_{nmp}. \tag{6}$$

A single matrix operating on the vector $\widetilde{\boldsymbol{\psi}}$ (all modal coefficients representing the given function) may then equivalently be considered as having block-elements which are other matrices. We always view the modal set for a function on a cylindrical or rectangular subdomain as a direct product of *three* one-dimensional sets. However, in the case of the spherical shells (J, H, and O), we sometimes view the set of modal coefficients as the direct product of only *two* sets, the set corresponding to the radial modes and the set corresponding to the spherical harmonic modes (which involve both the polar and azimuthal angles).

Operators corresponding to a single dimension, that is "simple" matrices (whose elements are numbers, not matrices), are usually represented by an ordinary-font capital, such as the identity operator/matrix I_X or the matrix D_Z which realizes differentiation by Z. Matrices which act on the full set of modal coefficients are represented by a calligraphic capital, for example $\mathcal{B}$. Thus, if $B_{Z[1]}$ represents integration in Z, then on a rectangular block we might use $\mathcal{B} = I_X \otimes I_Y \otimes B_{Z[1]}$ as the matrix which, when applied to a vector $\widetilde{\boldsymbol{\psi}}$ holding the full set of modal coefficients, realizes integration in Z with no action in X or Y. That is, if $\psi(X,Y,Z)$ has modal coefficients $\widetilde{\boldsymbol{\psi}}$, then formally $\int\psi(X,Y,Z)dZ$ has modal coefficients $\mathcal{B}\widetilde{\boldsymbol{\psi}}$. The [1] on $B_{Z[1]}$ indicates that all entries in its first row (the zeroth row by our conventions) are zero, so that $(\mathcal{B}\widetilde{\boldsymbol{\psi}})(\alpha) = 0$ whenever $p = 0$ for the index $\alpha = n(N_Y+1)(N_Z+1)+m(N_Z+1)+p$ (cf. Eq. (6)). This choice would fix the integration "constant" (a function of X and Y) in $\int\psi(X,Y,Z)dZ$, but these empty rows (labelled by m and n) might also be subsequently filled with "tau-conditions," that is nontrivial vectors chosen to fix a different "constant."

1.3.2. Integration preconditioning

We review the key ideas behind the technique of integration preconditioning, continuing to assume a rectangular block subdomain and also assuming the HRWE operator (4). Repeated use of the Leibniz rule casts (4) (again with tildes suppressed) into the form

$$L = \partial_Y^2 + \partial_X^2(1-\Omega^2Z^2) + \partial_Z^2(1-\Omega^2X^2) - \Omega^2(\partial_X X + \partial_Z Z - 2\partial_X\partial_Z XZ). \tag{7}$$

We view this equation as an *operator identity*; partial derivatives "see" both terms like Z^2 and XZ to the right, and also the function (not shown) on which L will eventually act. The $T_n(\xi)$ obey the three-term recurrence $2\xi T_n(\xi) = T_{n+1}(\xi) + T_{n-1}(\xi)$. Here ξ may be viewed as a suitable rescaling of either X, Y, or Z. Therefore, multiplication by the independent variable (for the moment ξ) is represented in the corresponding space of modal coefficients by a banded (evidently a tridiagonal) matrix A_ξ. In fact, multiplication by a polynomial $p(\xi)$ is similarly represented by a banded matrix $p(A_\xi)$. The matrix which represents L is

$$\mathcal{L} = I_X \otimes D_Y^2 \otimes I_Z + D_X^2 \otimes I_Y \otimes (I_Z - \Omega^2 A_Z^2) + (I_X - \Omega^2 A_X^2) \otimes I_Y \otimes D_Z^2 - \Omega^2 (D_X A_X \otimes I_Y \otimes I_Z + I_X \otimes I_Y \otimes D_Z A_Z - 2 D_X A_X \otimes I_Y \otimes D_Z A_Z), \tag{8}$$

where each D represents differentiation in the space of modal coefficients for one coordinate. Overall $\mathcal{L}$ is neither sparse nor banded, since these desirable features are spoiled by the derivative matrices (see the second paragraph of this subsection).

The idea behind integration preconditioning is to "undo" all matrix differentiations through repeated application of integration matrices (cf. point (iii) in the second paragraph of this subsection). To illustrate, we consider the modal representation $\mathcal{L}\tilde{\boldsymbol{\psi}} = \tilde{\mathbf{g}}$ of (3) on the block, ignoring boundary conditions for now. Introducing $\mathcal{B} \equiv B_{X[2]}^2 \otimes B_{Y[2]}^2 \otimes B_{Z[2]}^2$, we then form $\mathcal{B}\mathcal{L}\tilde{\boldsymbol{\psi}} = \mathcal{B}\tilde{\mathbf{g}}$. The coefficient matrix of the new "preconditioned" system is then

$$\mathcal{B}\mathcal{L} = B_{X[2]}^2 \otimes I_{Y[2]} \otimes B_{Z[2]}^2 + I_{X[2]} \otimes B_{Y[2]}^2 \otimes (B_{Z[2]}^2 - \Omega^2 B_{Z[2]}^2 A_Z^2) + (B_{X[2]}^2 - \Omega^2 B_{X[2]}^2 A_X^2) \otimes B_{Y[2]}^2 \otimes I_{Z[2]} - \Omega^2 (B_{X[2]} A_X \otimes B_{Y[2]}^2 \otimes B_{Z[2]}^2 + B_{X[2]}^2 \otimes B_{Y[2]}^2 \otimes B_{Z[2]} A_Z - 2 B_{X[2]} A_X \otimes B_{Y[2]}^2 \otimes B_{Z[2]} A_Z). \tag{9}$$

Built with Bs and As, this matrix is sparse and banded, albeit with large bandwidth.

The matrix $\mathcal{B}\mathcal{L}$ has many empty rows, signaling missing information. The spectral-tau procedure is to put the "tau conditions," here the boundary conditions, in these empty rows, and the corresponding inhomogeneous values in $\mathcal{B}\tilde{\mathbf{g}}$. When this procedure is carried out correctly, with due regard to possible repetition in the specification of boundary data, the empty rows provide precisely the space needed for the boundary data of a well-posed problem. To enforce boundary conditions for the example at hand, we proceed as follows. We define, for example, $h^+(X,Y) = \psi(X,Y,Z_{\max})$ and $h^-(X,Y) = \psi(X,Y,Z_{\min})$. Then Dirichlet boundary conditions along the XY-faces of a block are expressible as

$$\sum_{p=0}^{N_Z} \widetilde{\psi}_{nmp} \delta_p^{\pm} = \tilde{h}_{nm}^{\pm}, \tag{10}$$

where a double Chebyshev projection appears on the right-hand side. Moreover, δ^+ (all 1's) and δ^- (alternating $+1$ and -1) are the (N_Z+1) dimensional "Dirichlet vectors." Similar equations correspond to YZ and XY faces, and in all $2(N_X+1)(N_Y+1) + 2(N_Y+1)(N_Z+1) + 2(N_X+1)(N_Z+1)$ such equations are possible. This is more than the

$$2(N_X+1)(N_Y+1) + 2(N_Y+1)(N_Z+1) + 2(N_X+1)(N_Z+1) - 4(N_X+N_Y+N_Z+1)$$

available empty rows in (9). However, there are precisely $4(N_X+N_Y+N_Z+1)$ linear dependencies amongst the set of all possible boundary equations, owing to the fact that faces share common edge values. Table 1 gives our prescription for filling empty rows.

As a result of the integration preconditioning, we have reformulated the set of equations in terms of matrices with a drastic reduction in the number of nonzero elements. In the context of ODEs, that is in the 1D origins of this method, Ref. [1] has thoroughly studied the condition number of the resulting preconditioned matrix with respect to norms that arise from diagonal equilibration. While in the ODE context integration preconditioning often improves the conditioning of the original system, in the PDE context at hand the matrix $B_{X[2]}^2 \otimes B_{Y[2]}^2 \otimes B_{Z[2]}^2$ does not appear to be a beneficial preconditioner. Indeed, in comparison with the "unpreconditioned" matrix (8), the "preconditioned" matrix (9) would seem no closer to the identity (in fact, it is arguably farther from it). Regardless, *sparsification* is a desirable property, since it clearly affords a *fast* matrix–vector multiply in Krylov methods. Therefore, for multidimensional problems we are more comfortable focusing on the sparsifying aspect of the technique, with the understanding that *further preconditioning* (described below) on top of the "integration preconditioning" will be required to enhance convergence of the underlying linear solver (in our case GMRES).

2. Sparse spectral approximation of the 3d HRWE

This section describes the spectral-tau representation of L in (4) on each of the basic subdomains, except for the block case which we have already described in Section 1.3. These descriptions allow for implementation of the left-hand side of (3) as a "matrix–vector multiply," an implementation required by the iterative solver GMRES [33].

Table 1
Filling of empty rows for blocks.

Face	Rows	Index restrictions
$Z = Z_{\min}$	$n(N_Y+1)(N_Z+1) + m(N_Z+1) + 0$	$0 \leqslant n \leqslant N_X,\ 0 \leqslant m \leqslant N_Y$
$Z = Z_{\max}$	$n(N_Y+1)(N_Z+1) + m(N_Z+1) + 1$	$0 \leqslant n \leqslant N_X,\ 0 \leqslant m \leqslant N_Y$
$Y = Y_{\min}$	$n(N_Y+1)(N_Z+1) + p$	$0 \leqslant n \leqslant N_X,\ 2 \leqslant p \leqslant N_Z$
$Y = Y_{\max}$	$n(N_Y+1)(N_Z+1) + (N_Z+1) + p$	$0 \leqslant n \leqslant N_X,\ 2 \leqslant p \leqslant N_Z$
$X = X_{\min}$	$m(N_Z+1) + p$	$2 \leqslant m \leqslant N_Y,\ 2 \leqslant p \leqslant N_Z$
$X = X_{\max}$	$(N_Y+1)(N_Z+1) + m(N_Z+1) + p$	$2 \leqslant m \leqslant N_Y,\ 2 \leqslant p \leqslant N_Z$

2.1. Outer spherical shell

In the polar system associated with the comoving system (1) the operator (4) becomes

$$r^2 L = r^2\Delta - \Omega^2 J_O, \quad r^2\Delta = \partial_r^2 r^2 - 2\partial_r r + \Delta_{S^2}, \quad J_O = r^2\partial_\varphi^2, \tag{11}$$

where Δ_{S^2} is the unit-sphere Laplacian and O stands for the *outer* spherical shell. These equations should be viewed as operator identities acting on scalar functions. We approximate the solution ψ to $L\psi = g$ as the finite triple series

$$\begin{aligned}\mathcal{P}_{N_r,N_\theta}\psi(r,\theta,\varphi) = &\sum_{n=0}^{N_r}\sum_{\ell=0}^{N_\theta}\widetilde{\psi}_{\ell 0 n}\overline{P}_{\ell 0}(\cos\theta)T_n(\xi(r)) \\ &+\sum_{n=0}^{N_r}\sum_{\ell=1}^{N_\theta}\sum_{m=1}^{N_\theta}\overline{P}_{\ell m}(\cos\theta)\left[\widetilde{\psi}_{\ell,2m-1,n}\cos(m\varphi)+\widetilde{\psi}_{\ell,2m,n}\sin(m\varphi)\right]T_n(\xi(r)),\end{aligned} \tag{12}$$

where the $\overline{P}_{\ell m}(u)$ are normalized associated Legendre functions (denoted by $\overline{P}_\ell^m(u)$ in Ref. [35]) and $\xi(r)$ maps the radial domain to the standard interval $[-1,1]$.

We represent the triply-indexed modal coefficients $\widetilde{\psi}_{\ell qn}$ as a vector $\widetilde{\boldsymbol{\psi}}(\alpha)$ of length $(N_\theta+1)(2N_\theta+1)(N_r+1)$, with the two notations connected by

$$\widetilde{\boldsymbol{\psi}}(\ell(2N_\theta+1)(N_r+1)+q(N_r+1)+n) = \widetilde{\psi}_{\ell qn}. \tag{13}$$

For $\ell < N_\theta$ the sum over m in (12) includes too many terms. Indeed, m should run from 1 to ℓ only (the $m=0$ terms appear in the first sum); therefore, when $q > 2\ell$, we set $\widetilde{\psi}_{\ell qn} = 0$ by hand [see after Eq. (18)]. We have enlarged the space of modal coefficients for convenience when using spherical harmonic transformations. With this remark in mind, for our representation (13) the index α of the vector $\widetilde{\psi}(\alpha)$ takes on all values corresponding to the ranges $0 \leqslant \ell \leqslant N_\theta$, $0 \leqslant q \leqslant 2N_\theta$, and $0 \leqslant n \leqslant N_r$. We denote by $\mathbb{P}$ the projection matrix whose range is the set of vectors with proper spherical harmonic expansions,

$$(\mathbb{P}\widetilde{\boldsymbol{\psi}})(\ell(2N_\theta+1)(N_r+1)+q(N_r+1)+n) = 0, \quad \text{for } q > 2\ell. \tag{14}$$

Let us first consider a sparse approximation of the Laplacian term $r^2\Delta$, which from (11) has the spectral representation

$$\mathcal{A}_r^2\boldsymbol{\Delta} = \mathbb{P}\left[I_\theta\otimes I_\varphi\otimes\left(D_r^2A_r^2 - 2D_rA_r\right) - \mathscr{L}^2\otimes I_r\right], \tag{15}$$

where $\mathcal{A}_r^2 = I_\theta\otimes I_\varphi\otimes A_r^2$, and A_r is the matrix equivalent to multiplying r-dependent functions by a factor of r. In the first term within the square brackets $I_\theta\otimes I_\varphi\otimes$ implies that there are no operations mixing modes $\widetilde{\psi}_{\ell qn}$ with different values of ℓ, or of q (i.e. the dual indices to θ and ϕ). The operator $(D_r^2A_r^2 - 2D_rA_r)$ is the matrix equivalent of the partial differentiation $\partial_r^2 r^2 - 2\partial_r r$ in (11). The matrix $\mathscr{L}^2$, representing $-\Delta_{S^2}$ in (11), is comprised of $(N_\theta+1)$ constant blocks $\ell(\ell+1)I_{(2N_\theta+1)\times(2N_\theta+1)}$ in each subspace labeled by ℓ.

To get a sparse form of the Laplacian, we define $\mathcal{B} = I_\theta\otimes I_\varphi\otimes B_r^2$ and write the expression

$$(\mathcal{B}\mathcal{A}_r^2\boldsymbol{\Delta})^{\text{modified}} = \mathbb{P}\left[I_\theta\otimes I_\varphi\otimes(I_{r[2]}A_r^2 - 2B_{r[2]}A_r) - \mathscr{L}^2\otimes B_{r[2]}^2\right] + (I_\theta\otimes I_\varphi\otimes I_r - \mathbb{P}). \tag{16}$$

Here, "modified" indicates that, by addition of the last term above, 1's have been placed on the diagonal in rows set to zero by the projection operation. Finally, from (11) the sparse preconditioned form of the operator J_O is

$$\mathcal{B}\mathcal{J}_O = -\mathbb{P}\left[I_\theta\otimes\mathscr{M}^2\otimes B_{r[2]}^2A_r^2\right], \tag{17}$$

where $\mathscr{M}^2 = \text{diag}(0,1,1,4,4,\ldots,N_\theta^2,N_\theta^2)$ is the $(2N_\theta+1)$-by-$(2N_\theta+1)$ matrix representing $-\partial_\varphi^2$. Therefore, prior to inclusion of boundary conditions, our sparse form of the linear system for the other shell O is

$$\left[(\mathcal{B}\mathcal{A}_r^2\boldsymbol{\Delta})^{\text{modified}} - \Omega^2\mathcal{B}\mathcal{J}_O\right]\widetilde{\boldsymbol{\psi}} = \mathcal{B}\mathcal{A}_r^2\tilde{\mathbf{g}}. \tag{18}$$

Some of these equations are $\widetilde{\psi}_{\ell qn} = 0$ for $q > 2\ell$, since we demand that the spectral representation $\tilde{\mathbf{g}}$ of the inhomogeneous source obeys $\tilde{\mathbf{g}} = \mathbb{P}\tilde{\mathbf{g}}$.

We now consider radiation conditions on ∂O^+, summarizing results given in [6]. Specification of Dirichlet (or of matching) conditions on the inner boundary ∂O^- is essentially the same issue described in detail below for the boundaries of an inner shell. To specify the radiation conditions on ∂O^+, we set $R = r_{\max}$, the radial coordinate value of ∂O^+, and introduce

$$V_{\ell+1/2}(\xi) = \sqrt{\frac{\pi\xi}{2}}\exp\left[-\mathrm{i}\left(\xi - \frac{1}{2}\pi\ell - \frac{1}{2}\pi\right)\right]H_{\ell+1/2}^{(+)}(\xi), \tag{19}$$

which satisfies $V_{\ell+1/2}(\xi)\sim 1$ as $\xi\to\infty$. Here $H_{\ell+1/2}^{(+)}(\xi)$ is the cylindrical Hankel function of the first kind, of half-integer order $\ell+1/2$. For our radiative boundary condition we will need the "frequency–domain kernel,"

$$v_{\ell+1/2}(\xi) \equiv \xi\,\frac{V'_{\ell+1/2}(\xi)}{V_{\ell+1/2}(\xi)}, \tag{20}$$

which is computable as a continued fraction via Steed's algorithm [37]. Radiation conditions involve

$$\kappa_{\ell m} \equiv m\Omega R + \mathrm{Im}\big(\nu_{\ell+1/2}(m\Omega R)\big), \quad \lambda_{\ell m} \equiv 1 - \mathrm{Re}\big(\nu_{\ell+1/2}(m\Omega R)\big), \tag{21}$$

with $\kappa_{\ell 0} = 0$ and $\lambda_{m0} = \ell + 1$ for $m = 0$ modes. (Ref. [6] used p and q for $\kappa_{\ell m}$ and $\lambda_{\ell m}$, but we do not use that notation here in order to avoid confusion with the indices on $\widetilde{\psi}_{\ell q n}$.) As tau-conditions, our radiation conditions are then expressible as

$$\sum_{n=0}^{N_r}\Big(R\widetilde{\psi}_{\ell,2m,n}\nu_n^+ + \kappa_{\ell m}\widetilde{\psi}_{\ell,2m-1,n}\delta_n^+ + \lambda_{\ell m}\widetilde{\psi}_{\ell,2m,n}\delta_n^+\Big) = 0 \tag{22a}$$

$$\sum_{n=0}^{N_r}\Big(R\widetilde{\psi}_{\ell,2m-1,n}\nu_n^+ - \kappa_{\ell m}\widetilde{\psi}_{\ell,2m,n}\delta_n^+ + \lambda_{\ell m}\widetilde{\psi}_{\ell,2m-1,n}\delta_n^+\Big) = 0. \tag{22b}$$

Here δ^+ (all 1's) and δ^- (alternating $+1$ and -1) are the (N_r+1) dimensional "Dirichlet vectors" used to impose Dirichlet conditions at the endpoints of a coordinate range. Similarly, ν^+ and ν^- are the (N_r+1) dimensional "Neumann vectors" used to impose derivative conditions at the endpoints. Details are given in [1,6].

Along the block-diagonal of the matrix $(\mathcal{B}\mathcal{A}_r^2\mathbf{\Lambda})^{\text{modified}} - \Omega^2\mathcal{B}\mathcal{J}_0$, there are (N_r+1)-by-(N_r+1) blocks, one for each (ℓ, q) pair. When q exceeds 2ℓ, each such block is the identity matrix; however, the block corresponding to a physical mode $0 \leqslant q \leqslant 2\ell$ has the form

$$\left[\begin{array}{c} \mathbf{0} \\ \mathbf{0} \\ \hline \mathsf{B}^{\ell q} \end{array}\right]. \tag{23}$$

Here $\mathbf{0}$ represents a row of zeros, and $\mathsf{B}^{\ell q}$ is a nonzero (N_r-1)-by-(N_r+1) submatrix (here we use *superscripts* ℓ and q to label matrices). The zeros in the first two rows are filled in with the Dirichlet boundary conditions on ∂O^-, using δ^-, and the radiation boundary conditions on ∂O^+, using (22). Since these radiation conditions mix one cosine ($q = 2m-1$) and the other sine ($q = 2m$) mode, the tau conditions lead to a coupling between the blocks. The resulting $2(N_r+1)$-by-$2(N_r+1)$ block neighborhood, with Dirichlet and radiation boundary conditions, takes one of the following forms (either representation is possible due to the homogeneity of the boundary conditions):

$$\left[\begin{array}{c|c} \delta^- & 0 \\ \kappa_{\ell m}\delta^+ & R\nu^+ + \lambda_{\ell m}\delta^+ \\ \mathsf{B}^{\ell,2m-1} & 0 \\ \hline 0 & \delta^- \\ R\nu^+ + \lambda_{\ell m}\delta^+ & -\kappa_{\ell m}\delta^+ \\ 0 & \mathsf{B}^{\ell,2m} \end{array}\right] \quad \text{or} \quad \left[\begin{array}{c|c} \delta^- & 0 \\ R\nu^+ + \lambda_{\ell m}\delta^+ & -\kappa_{\ell m}\delta^+ \\ \mathsf{B}^{\ell,2m-1} & 0 \\ \hline 0 & \delta^- \\ \kappa_{\ell m}\delta^+ & R\nu^+ + \lambda_{\ell m}\delta^+ \\ 0 & \mathsf{B}^{\ell,2m} \end{array}\right], \tag{24}$$

where $\mathbf{0}$ represents either a row (when opposite a δ^-) or a (N_r-1)-by-(N_r+1) submatrix of zeros (when opposite a B). Boundary conditions for $m = 0$ correspond to blocks

$$\left[\begin{array}{c} \delta^- \\ R\nu^+ + \lambda_{\ell 0}\delta^+ \\ \hline \mathsf{B}^{\ell 0} \end{array}\right]. \tag{25}$$

Evidently, for "zero modes" only a single azimuthal block need be considered.

2.2. Inner spherical shells

We assume that one of the "holes" is at $\widetilde{Z} = z_H$ and define new comoving coordinates

$$z = \widetilde{Z} - z_H, \quad x = \widetilde{X}, \quad y = \widetilde{Y}. \tag{26}$$

The helically reduced wave operator (4) in the new coordinates is

$$L = \frac{\partial^2}{\partial x^2} + \frac{\partial^2}{\partial y^2} + \frac{\partial^2}{\partial z^2} - \Omega^2\left[(z_H + z)\frac{\partial}{\partial x} - x\frac{\partial}{\partial z}\right]^2. \tag{27}$$

Spherical polar coordinates $\{r, \theta, \phi\}$ in this subsection correspond to the $\{x, y, z\}$ system which is not the comoving system $\{\widetilde{x}, \widetilde{y}, \widetilde{z}\}$ in (1). Therefore, $\{r, \theta, \phi\}$ is not the system $\{r, \theta, \varphi\}$ corresponding to the outer shell, although only the notation for the azimuthal angle (ϕ vs φ) reflects the difference. Nevertheless, for an inner shell our treatment of the Laplacian part of the operator is the same as the treatment given in the last subsection. In particular, we adopt the same conventions for the indexing of the spectral representation, and therefore again arrive at the expression (16). Notationally, the only difference is that we replace all instances of φ with ϕ. Therefore, having already considered $(r^2\times)$ the Laplacian part of the HRWE, we turn to $(r^2\times)$ the term in (27) paired with $-\Omega^2$,

$$J_H \equiv r^2[(z_H + z)\partial/\partial x - x\partial/\partial z]^2. \tag{28}$$

To facilitate the expression of (28) in terms of $\{r,\theta,\phi\}$, we introduce

$$Q = \sin\theta\cos\phi \tag{29}$$
$$P = \cos\theta\cos\phi\,\partial/\partial\theta - \csc\theta\sin\phi\,\partial/\partial\phi \tag{30}$$
$$N = \cos\phi\,\partial/\partial\theta - \cos\theta\csc\theta\sin\phi\,\partial/\partial\phi \tag{31}$$

and note that

$$\partial/\partial x = Q\partial/\partial r + r^{-1}P, \quad z\partial/\partial x - x\partial/\partial z = N. \tag{32}$$

With the identities (which should be read as operators acting on a scalar function)

$$r^2\partial_r^2 = \partial_r^2 r^2 - 4\partial_r r + 2, \quad r\partial_r = \partial_r r - 1, \quad r^2\partial_r = \partial_r r^2 - 2r, \tag{33}$$

we then find that J_H in (28) can be written as

$$J_H = z_H^2 Q^2\partial_r^2 r^2 + z_H^2(PQ + QP - 4Q^2)\partial_r r + z_H(NQ + QN)\partial_r r^2 + z_H(NP + PN - 2NQ - 2QN)r + N^2 r^2 + z_H^2(P^2 + 2Q^2 - PQ - 2QP). \tag{34}$$

We use $\mathcal{J}_H$ to denote the spectral form of the differential operator J_H. The corresponding sparse form $\mathcal{B}\mathcal{J}_H \equiv (I_\theta \otimes I_\phi \otimes B^2_{r[2]})\mathcal{J}_H$ is then

$$\mathcal{B}\mathcal{J}_H = z_H^2\mathsf{Q}^2 \otimes I_{r[2]}A_r^2 + z_H^2(\mathsf{PQ} + \mathsf{QP} - 4\mathsf{Q}^2) \otimes B_{r[2]}A_r + z_H(\mathsf{NQ} + \mathsf{QN}) \otimes B_{r[2]}A_r^2 + z_H(\mathsf{NP} + \mathsf{PN} - 2(\mathsf{NQ} + \mathsf{QN})) \otimes B^2_{r[2]}A_r + \mathsf{N}^2 \otimes B^2_{r[2]}A_r^2 + z_H^2(\mathsf{P} - 2\mathsf{Q})(\mathsf{P} - \mathsf{Q}) \otimes B^2_{r[2]}. \tag{35}$$

N, P, and Q (san serif font) are matrices acting on the spectral space of spherical harmonic expansion coefficients, as described below. We compute the matrices appearing in (35) as truncations of the corresponding infinite dimensional matrices (so products like PQ etc. are computed before truncation). The components $\mathsf{N}(\alpha,\beta)$ of N obey the following condition:

$$\mathsf{N}(\ell(2N_\theta + 1) + q, k(2N_\theta + 1) + p) = 0, \quad \text{for } q > 2\ell \quad \text{or} \quad p > 2k \tag{36}$$

and similarly for the components $\mathsf{P}(\alpha,\beta)$ and $\mathsf{Q}(\alpha,\beta)$. (Here we have switched to parenthesis notation [34] for the components $\mathsf{N}(\alpha,\beta) = \mathsf{N}_{\alpha\beta}$ of a matrix.) This condition reflects the extraneous components we have included in our expansion vector $\tilde{\psi}$.

We first sketch how N stems from the action of N on spherical harmonics. Using standard formulas from the theory of angular momentum (see the appendix of [37]), we find

$$NY_{\ell m} = \frac{1}{2}\sqrt{(\ell - m)(\ell + m + 1)}Y_{\ell,m+1} - \frac{1}{2}\sqrt{(\ell + m)(\ell - m + 1)}Y_{\ell,m-1}. \tag{37}$$

Before turning to the construction of N, we relate the complex representation of spherical harmonics $Y_{\ell m}(\theta,\phi)$ to the real-valued representation. Since

$$Y_{\ell m}(\theta,\phi) = \sqrt{\frac{1}{2\pi}}(-1)^m\overline{P}_{\ell m}(\cos\theta)e^{\mathrm{i}m\phi}, \quad Y_{\ell,-m}(\theta,\phi) = \sqrt{\frac{1}{2\pi}}\overline{P}_{\ell m}(\cos\theta)e^{-\mathrm{i}m\phi}, \quad 0 \leqslant m \leqslant \ell \tag{38}$$

for fixed ℓ an expansion in the azimuthal index can take either of the following forms:

$$c_{\ell 0}Y_{\ell 0} + \sum_{m=1}^{\ell}(c_{\ell m}Y_{\ell m} + c_{\ell,-m}Y_{\ell,-m}) = a_{\ell 0}\overline{P}_{\ell 0} + \sum_{m=1}^{\ell}\overline{P}_{\ell m}[a_{\ell,2m-1}\cos m\phi + a_{\ell,2m}\sin m\phi], \tag{39}$$

where the real expansion coefficients $a_{\ell q}$ are given by $\sqrt{2\pi}a_{\ell 0} = c_{\ell 0}$ and

$$\sqrt{2\pi}a_{\ell,2m-1} = c_{\ell m}(-1)^m + c_{\ell,-m}, \quad \sqrt{2\pi}a_{\ell,2m} = \mathrm{i}\big[c_{\ell m}(-1)^m - c_{\ell,-m}\big], \quad 1 \leqslant m \leqslant \ell. \tag{40}$$

For $a_{\ell q}$ the physical range of q is $q = 0,\ldots,2\ell$ (as mentioned, in practice this range is extended to $q = 0,\ldots,2N_\theta$). We define another set of complex expansion coefficients

$$f_{\ell m} = \frac{1}{2}\sqrt{(\ell + m)(\ell - m + 1)}c_{\ell,m-1} - \frac{1}{2}\sqrt{(\ell - m)(\ell + m + 1)}c_{\ell,m+1}, \tag{41}$$

so that from (37) the action of N has the effect

$$\Psi = \sum_{\ell=0}^{\infty}\sum_{m=-\ell}^{\ell}c_{\ell m}Y_{\ell m}, \quad N\Psi = \sum_{\ell=0}^{\infty}\sum_{m=-\ell}^{\ell}f_{\ell m}Y_{\ell m}. \tag{42}$$

We can represent N by the matrix that converts the vector of coefficients $c_{\ell m}$ to the vector $f_{\ell m}$. Correspondingly, with $d_{\ell q}$ related to $f_{\ell m}$ in the same way $a_{\ell q}$ are related to $c_{\ell m}$, we view the action of N as a mapping from the real coefficients $a_{\ell q}$ to the real coefficients $d_{\ell q}$.

Similarly, expressions for Q and P following from the identities

$$QY_{\ell m} = \frac{1}{2}\sqrt{\frac{(\ell-m+1)(\ell-m+2)}{(2\ell+1)(2\ell+3)}}Y_{\ell+1,m-1} - \frac{1}{2}\sqrt{\frac{(\ell+m+1)(\ell+m+2)}{(2\ell+1)(2\ell+3)}}Y_{\ell+1,m+1}$$
$$-\frac{1}{2}\sqrt{\frac{(\ell+m)(\ell+m-1)}{(2\ell+1)(2\ell-1)}}Y_{\ell-1,m-1} + \frac{1}{2}\sqrt{\frac{(\ell-m)(\ell-m-1)}{(2\ell+1)(2\ell-1)}}Y_{\ell-1,m+1}, \tag{43}$$

$$PY_{\ell m} = -\frac{1}{2}\ell\sqrt{\frac{(\ell-m+1)(\ell-m+2)}{(2\ell+1)(2\ell+3)}}Y_{\ell+1,m-1} + \frac{1}{2}\ell\sqrt{\frac{(\ell+m+1)(\ell+m+2)}{(2\ell+1)(2\ell+3)}}Y_{\ell+1,m+1}$$
$$-\frac{1}{2}(\ell+1)\sqrt{\frac{(\ell+m)(\ell+m-1)}{(2\ell+1)(2\ell-1)}}Y_{\ell-1,m-1} + \frac{1}{2}(\ell+1)\sqrt{\frac{(\ell-m)(\ell-m-1)}{(2\ell+1)(2\ell-1)}}Y_{\ell-1,m+1}, \tag{44}$$

which again stem from results tabulated in the appendix of [37].

To enforce the inner and outer boundary conditions in (3), we fill empty rows in $(\mathcal{B}\mathcal{A}_r^2\Delta)^{\text{modified}} - \Omega^2\mathcal{B}\mathcal{J}_H$ with the tau-conditions. Let $h^+(\theta,\phi) = \psi(r_{\max},\theta,\phi)$ and $h^-(\theta,\phi) = \psi(r_{\min},\theta,\phi)$. Then Dirichlet boundary conditions on the inner and outer boundaries of the shell are expressible as

$$\sum_{n=0}^{N_r}\widetilde{\psi}_{\ell qn}\delta_n^{\pm} = \tilde{h}_{\ell q}^{\pm}, \tag{45}$$

where spherical-harmonic projections appear on the right-hand side. Table 2 shows how empty rows are filled to enforce these boundary conditions.

2.3. Cylindrical shells

Throughout this section we suppress the tildes on $\widetilde{X},\widetilde{Y},\widetilde{Z}$. Let $\rho = (X^2+Y^2)^{1/2}$, and multiply Eq. (4) by ρ^2 to get the operator identity

$$\rho^2 L = \rho^2\left[\partial_Y^2 + \partial_X^2 + \partial_Z^2 - \Omega^2\partial_X^2 Z^2 - \Omega^2\partial_Z^2 X^2 - \Omega^2(\partial_X X + \partial_Z Z - 2\partial_X X\partial_Z Z)\right]. \tag{46}$$

Since $X = \rho\cos\phi$ and $Y = \rho\sin\phi$,

$$\rho^2(\partial_X^2 + \partial_Y^2 + \partial_Z^2) = \partial_\rho^2\rho^2 - 3\partial_\rho\rho + 1 + \partial_\phi^2 + \rho^2\partial_Z^2, \tag{47}$$

again with the view that this is an operator identity. Eq. (47) has the spectral representation

$$\mathcal{A}_\rho^2\mathbf{\Delta} = I_\phi\otimes(I_\rho + D_\rho^2 A_\rho^2 - 3D_\rho A_\rho)\otimes I_Z + D_\phi^2\otimes I_\rho\otimes I_Z + I_\phi\otimes A_\rho^2\otimes D_Z^2. \tag{48}$$

Here $\mathcal{A}_\rho^2$ represents the matrix $I_\phi\otimes A_\rho^2\otimes I_Z$. To achieve this representation we start by introducing a mapping of $[Z_{\min},Z_{\max}]$ to $[-1,1]$ with the function $\chi(Z)$, so that Z dependence can be expressed with the Chebyshev polynomials $T_p(\chi(Z))$. Similarly $\xi(\rho)$ maps $[\rho_{\min},\rho_{\max}]$ to $[-1,1]$. The solution is then approximated as (taking N_ϕ even for simplicity)

$$\mathcal{P}_{N_\rho,N_\phi,N_z}\psi(\rho,\phi,Z) = \sum_{n=0}^{N_\rho}\sum_{p=0}^{N_z}\widetilde{\psi}_{0np}T_n(\xi(\rho))T_p(\chi(Z)) + \sum_{k=1}^{\frac{1}{2}N_\phi}\sum_{n=0}^{N_\rho}\sum_{p=0}^{N_z}\left[\widetilde{\psi}_{2k-1,np}\cos(k\phi) + \widetilde{\psi}_{2k,np}\sin(k\phi)\right]T_n(\xi(\rho))T_p(\chi(Z)). \tag{49}$$

The direct product structure in (48) has been determined by the convention

$$\widetilde{\psi}(m(N_\rho+1)(N_z+1) + n(N_z+1) + p) = \widetilde{\psi}_{mnp}. \tag{50}$$

We "sparsify" the matrix representation (48) via multiplication by $\mathcal{B} = B_\phi^2\otimes B_{\rho[2]}^2\otimes B_{Z[2]}^2$. In this operator the $B_{\rho[2]}^2$ and $B_{Z[2]}^2$ correspond to the usual B operators representing integration twice over a coordinate, and leaving two empty rows to be filled by tau-conditions. The operator B_ϕ^2 is associated with a periodic coordinate, and hence no applicable boundary conditions. It represents double integration over all Fourier modes except the zero mode, which is left unchanged. The matrix that accomplishes this has the explicit form $B_\phi^2 = \text{diag}(1,-1,-1,-\frac{1}{4},-\frac{1}{4},-\frac{1}{9},-\frac{1}{9},\cdots)$. Although B_ϕ^2 does not play a role in handling boundary conditions, its application should further enhance spectrum clustering.

With this $\mathcal{B}$ sparsification of (48) yields

Table 2
Filling of empty rows for shells.

Boundary	Rows	Index restrictions
$r = r_{\min}$	$\ell(2N_\theta+1)(N_r+1) + q(N_r+1) + 0$	$0\leqslant\ell\leqslant N_\theta,\ 0\leqslant q\leqslant 2\ell$
$r = r_{\max}$	$\ell(2N_\theta+1)(N_r+1) + q(N_r+1) + 1$	$0\leqslant\ell\leqslant N_\theta,\ 0\leqslant q\leqslant 2\ell$

Table 3
Filling of empty rows for cylinders.

Boundary	Rows	Index restrictions
$\rho=\rho_{\min}$	$m(N_\rho+1)(N_z+1)+p$	$0\leqslant m\leqslant N_\phi,\ 2\leqslant p\leqslant N_z$
$\rho=\rho_{\max}$	$m(N_\rho+1)(N_z+1)+(N_z+1)+p$	$0\leqslant m\leqslant N_\phi,\ 2\leqslant p\leqslant N_z$
$Z=Z_{\min}$	$m(N_\rho+1)(N_z+1)+n(N_z+1)+0$	$0\leqslant n\leqslant N_\rho,\ 0\leqslant m\leqslant N_\phi$
$Z=Z_{\max}$	$m(N_\rho+1)(N_z+1)+n(N_z+1)+1$	$0\leqslant n\leqslant N_\rho,\ 0\leqslant m\leqslant N_\phi$

$$\mathcal{B}\mathcal{A}_\rho^2\mathbf{\Delta}=B_\phi^2\otimes(B_{\rho[2]}^2+I_{\rho[2]}A_\rho^2-3B_{\rho[2]}A_\rho)\otimes B_{Z[2]}^2+I_{\phi[1]}\otimes B_{\rho[2]}^2\otimes B_{Z[2]}^2+B_\phi^2\otimes B_{\rho[2]}^2A_\rho^2\otimes I_{Z[2]}. \tag{51}$$

Our analysis of the terms in the HRWE proportional to Ω^2 starts with the operator identities

$$\rho^2\partial_X X=\partial_\rho\rho^3\cos^2\phi-\rho^2(\cos^2\phi+\partial_\phi\cos\phi\sin\phi) \tag{52a}$$

$$\rho^2\partial_X^2=(\partial_\rho^2\rho^2-3\partial_\rho\rho+1)\cos^2\phi-\partial_\rho\rho(1-2\cos^2\phi+2\partial_\phi\cos\phi\sin\phi)+\partial_\phi^2\sin^2\phi+2\sin^2\phi-1, \tag{52b}$$

which follow from the chain and product rules. We have chosen the first term on the right-hand side of (52b) to match a similar term in the Laplacian part of the operator (cf. Eq. (47)).

We split the HRWE operator (46) on a cylindrical shell as $\rho^2L=\rho^2\Delta-\Omega^2J$, where

$$J=J_1+J_2+J_3+J_4=\underbrace{\rho^2\partial_X X(1-2\partial_Z Z)}_{J_1}+\underbrace{\rho^2\partial_X^2Z^2}_{J_2}+\underbrace{\rho^2\partial_Z Z}_{J_3}+\underbrace{\rho^2\partial_Z^2X^2}_{J_4}. \tag{53}$$

The piece $\rho^2\Delta$ was shown to lead to (51). We now focus on J whose matrix representation stems from the representations of its constituents. Eqs. (52a,b) give us

$$\mathrm{J}_1=C_\phi^2\otimes D_\rho A_\rho^3\otimes(I_Z-2D_ZA_Z)-(C_\phi^2+D_\phi C_\phi S_\phi)\otimes A_\rho^2\otimes(I_Z-2D_ZA_Z), \tag{54}$$

$$\mathrm{J}_2=C_\phi^2\otimes(I_\rho+D_\rho^2A_\rho^2-3D_\rho A_\rho)\otimes A_Z^2-(I_\phi-2C_\phi^2+2D_\phi C_\phi S_\phi)\otimes D_\rho A_\rho\otimes A_Z^2+(D_\phi^2S_\phi^2+2S_\phi^2-I_\phi)\otimes I_\rho\otimes A_Z^2, \tag{55}$$

$$\mathrm{J}_3=I_\phi\otimes A_\rho^2\otimes D_ZA_Z, \tag{56}$$

$$\mathrm{J}_4=C_\phi^2\otimes A_\rho^4\otimes D_Z^2, \tag{57}$$

where S_ϕ and C_ϕ are respectively the matrices in the Fourier basis which correspond to multiplication by $\sin\phi$ and $\cos\phi$. Application of the sparsifier $\mathcal{B}=B_\phi^2\otimes B_{\rho[2]}^2\otimes B_{Z[2]}^2$ yields

$$\mathcal{B}\mathrm{J}_1=B_\phi^2C_\phi^2\otimes B_{\rho[2]}A_\rho^3\otimes(B_{Z[2]}^2-2B_{Z[2]}A_Z)-(B_\phi^2C_\phi^2+B_{\phi[1]}C_\phi S_\phi)\otimes B_{\rho[2]}^2A_\rho^2\otimes(B_{Z[2]}^2-2B_{Z[2]}A_Z), \tag{58}$$

$$\begin{aligned}\mathcal{B}\mathrm{J}_2=&B_\phi^2C_\phi^2\otimes(B_{\rho[2]}^2+I_{\rho[2]}A_\rho^2-3B_{\rho[2]}A_\rho)\otimes B_{Z[2]}^2A_Z^2-(B_\phi^2-2B_\phi^2C_\phi^2+2B_{\phi[1]}C_\phi S_\phi)\otimes B_{\rho[2]}A_\rho\otimes B_{Z[2]}^2A_Z^2\\&+(I_{\phi[1]}S_\phi^2+2B_\phi^2S_\phi^2-B_\phi^2)\otimes B_{\rho[2]}^2\otimes B_{Z[2]}^2A_Z^2,\end{aligned} \tag{59}$$

$$\mathcal{B}\mathrm{J}_3=B_\phi^2\otimes B_{\rho[2]}^2A_\rho^2\otimes B_{Z[2]}A_Z, \tag{60}$$

$$\mathcal{B}\mathrm{J}_4=B_\phi^2C_\phi^2\otimes B_{\rho[2]}^2A_\rho^4\otimes I_{Z[2]}. \tag{61}$$

The sparsified matrix representing (46) is then $\mathcal{B}\mathcal{A}_\rho^2\mathcal{L}=\mathcal{B}\mathcal{A}_\rho\mathbf{\Delta}-\Omega^2(\mathcal{B}\mathrm{J}_1+\mathcal{B}\mathrm{J}_2+\mathcal{B}\mathrm{J}_3+\mathcal{B}\mathrm{J}_4)$.

To enforce boundary conditions, we fill empty rows in the matrix $\mathcal{B}\mathcal{A}_\rho\mathbf{\Delta}-\Omega^2\mathcal{B}\mathrm{J}$ with the tau-conditions. Let $h^+(\phi,Z)=\psi(\rho_{\max},\phi,Z)$, $h^-(\phi,Z)=\psi(\rho_{\min},\phi,Z)$ and $f^+(\rho,\phi)=\psi(\rho,\phi,Z_{\max})$, $f^-(\rho,\phi,Z_{\min})=\psi(\rho,\phi,Z_{\min})$. Then Dirichlet boundary conditions on the inner and outer axial boundaries and on the top and bottom caps are expressible as

$$\sum_{n=0}^{N_\rho}\widetilde{\psi}_{mnp}\delta_n^\pm=\tilde{h}_{mp}^\pm,\quad \sum_{p=0}^{N_z}\widetilde{\psi}_{mnp}\delta_p^\pm=\tilde{f}_{mn}^\pm. \tag{62}$$

There are $(N_\phi+1)(N_z+1)+(N_\rho+1)(N_\phi+1)$ such equations possible. However, owing to the fact that the caps shares common edges with both the inner and outer axial boundaries, there are $2(N_\phi+1)$ linear dependencies amongst these equations, and in fact the number of available empty rows is precisely $(N_\phi+1)(N_Z+1)+(N_\rho+1)(N_\phi+1)-2(N_\phi+1)$. Table 3 shows how we fill zero rows to enforce the boundary conditions.

3. Gluing of subdomains

So far we have described individual subdomains as if they were decoupled. We refer to the process of making them parts of a single problem as "gluing." Gluing, or matching, must be done for each subset of subdomains that touch, whether that touching is a finite volume overlap or a lower-dimensional shared boundary. The global problem requires matching for the following subdomain configurations: (i) two adjacent cylinders, (ii) one inner shell and a combination of cylinders and blocks, (iii) one cylinder and one block, and (iv) the outer shell O and the combination of blocks B and D and all cylinders.

We describe (i) and (ii) in detail, provide a sketch of (iii), and omit a description of (iv) altogether. Although more complicated, a description of (iv) would parallel that of (iii).

Before giving details, we comment on how gluing is reflected in the overall linear system. Let, for example, $\widetilde{\boldsymbol{\psi}}^J$ and $\widetilde{\boldsymbol{\psi}}^B$ respectively represent the vectors of modal coefficients belonging to the shell J and block B of Fig. 1. The overall set of unknowns is the concatenation

$$\widetilde{\boldsymbol{\Psi}} = (\widetilde{\boldsymbol{\psi}}^J, \widetilde{\boldsymbol{\psi}}^H, \widetilde{\boldsymbol{\psi}}^B, \widetilde{\boldsymbol{\psi}}^C, \widetilde{\boldsymbol{\psi}}^D, \widetilde{\boldsymbol{\psi}}^1, \widetilde{\boldsymbol{\psi}}^2, \widetilde{\boldsymbol{\psi}}^3, \widetilde{\boldsymbol{\psi}}^4, \widetilde{\boldsymbol{\psi}}^5, \widetilde{\boldsymbol{\psi}}^O)^t,$$

which satisfies a linear system stemming from Eq. (3),

$$\mathcal{M}\widetilde{\boldsymbol{\Psi}} = \mathcal{B}\widetilde{\mathcal{G}}, \tag{63}$$

with $\widetilde{\mathcal{G}}$ the concatenation of the sources on the subdomains. $\mathcal{B}$ indicates integration "preconditioning" (sparsification) on all subdomains. The coefficient matrix $\mathcal{M}$ is $\mathcal{BL}$, with $\mathcal{L}$ now the spectral representation of the HRWE operator L on the whole 2-center domain. This symbolic view ignores multiplications by radial powers on spheres and cylinders.

Each subdomain in Fig. 1 is represented by one of eleven super-blocks (J-J, H-H, $\cdots$, O-O) which sit along the diagonal of $\mathcal{M}$ representing the PDE on the whole 2-center domain. Here "super-block" is synonymous with "subdomain-block". The supplementary equations needed for gluing are placed within existing empty rows in the same manner as for the tau-conditions. However, the gluing conditions stretch beyond the super-block diagonal, since they are linear relationships between the spectral expansion coefficients on two (or more) separate subdomains. For example, the gluing together of cylinders 1 and 2 (which share a common cap) involves not only filling rows within the 1–1 and 2–2 super-blocks along the diagonal of $\mathcal{M}$, but also filling rows within the 1–2 and 2–1 off-diagonal super-blocks.

3.1. Gluing of cylinders to cylinders

As a specific example, let us consider the gluing of cylinders 1 and 2 in Fig. 1, which as indicated share the cap at $Z = Z_*$, where Z_* is $Z_{\max}$ for cylinder 1 and $Z_{\min}$ for cylinder 2 (the common cap has a hole in the middle, since 1 and 2 are cylindrical shells). Let, for example, $\mathcal{P}\psi^1$ be shorthand for the numerical solution $\mathcal{P}_{N^1_\rho, N^1_\phi, N^1_Z}\psi^1$ for cylinder 1, as expressed in (49). The restriction $\mathcal{P}\psi^1(\rho,\phi,Z_*)$ is a two-variable function on the cap $Z = Z_*$, and it can be expanded in a finite Fourier–Chebyshev series, with $\sum_{k=0}^{N^1_Z}\widetilde{\psi}^1_{qnk}\delta^+_k$ as the corresponding two-index modal coefficients. Likewise, the restriction $(d\mathcal{P}\psi^1/dZ)(\rho,\phi,Z_*)$ of the Z-derivative has a Fourier–Chebyshev series with two-index modal coefficients $\sum_{k=0}^{N^1_Z}\widetilde{\psi}^1_{qnk}\alpha_1 v^+_k$. The α_1 factor is a scaling of the Neumann vector v^+, and its presence is necessary since the range of Z is not $[-1,1]$ (details are given in [6]).

On the $Z = Z_*$ cap we likewise consider the numerical solution $\mathcal{P}\psi^2(\rho,\phi,Z_*)$ and its Z-derivative $(d\mathcal{P}\psi^2/dZ)(\rho,\phi,Z_*)$, as determined by the numerical solution $\mathcal{P}\psi^2$ on cylinder 2. We distinguish between two cases: (i) both the N_ρ and N_ϕ truncations are the same for cylinders 1 and 2 (but $N^1_Z \neq N^2_Z$ is allowed), and (ii) at least one of these truncations differs between the two cylinders (i.e., either $N^1_\rho \neq N^2_\rho$ or $N^1_\phi \neq N^2_\phi$, or both, hold). Let us first consider case (i), returning to case (ii) in the next paragraph. For case (i) both $\mathcal{P}\psi^1(\rho,\phi,Z_*)$ and $\mathcal{P}\psi^2(\rho,\phi,Z_*)$ have two-surface modes which are in one-to-one correspondence, and likewise for the derivatives. Therefore, for this case we enforce[2]

$$\sum_{k=0}^{N^1_Z}\widetilde{\psi}^1_{qnk}\delta^+_k = \sum_{k=0}^{N^2_Z}\widetilde{\psi}^2_{qnk}\delta^-_k, \quad \sum_{k=0}^{N^1_Z}\widetilde{\psi}^1_{qnk}\alpha_1 v^+_k = \sum_{k=0}^{N^2_Z}\widetilde{\psi}^2_{qnk}\alpha_2 v^-_k \tag{64}$$

for each Fourier–Chebyshev index pair (q,n). Here, for case (i), the matching conditions enforce continuity between the finite representations $\mathcal{P}\psi^1$ and $\mathcal{P}\psi^2$ across the cap, and also continuity between the finite representations $d\mathcal{P}\psi^1/dZ$ and $d\mathcal{P}\psi^2/dZ$. These matching conditions are reflected in the overall matrix $\mathcal{M}$ as follows. As the super-block corresponding to each of the subdomains 1 and 2 has been sparsified in the described fashion, each has a collection of empty rows which are also empty throughout $\mathcal{M}$. In, say, the empty rows stretching across the 1–1 and 1–2 super-blocks, we insert the first set of conditions given in (64). In the empty rows stretching across the 2–2 and 2–1 super-blocks, we similarly place the Neumann conditions, the second set of conditions given in (64). This filling of empty rows to achieve the required matching consists of relationships of modal coefficients with no reference to any "sources"; they are homogeneous equations.

To better understand the issues which will arise in matching volume-overlapping subdomains, we now consider case (ii), the case in which the cylinders 1 and 2 give rise to a disparate set of surface modes on the $Z = Z_*$ cap. In this case, for example, we again have $\sum_{k=0}^{N^1_Z}\widetilde{\psi}^1_{qnk}\delta^+_k$ as the modal coefficients determining $\mathcal{P}\psi^1(\rho,\phi,Z_*)$, and $\sum_{k=0}^{N^2_Z}\widetilde{\psi}^2_{qnk}\alpha_2 v^-_k$ as the modal coefficients determining $(d\mathcal{P}\psi^2/dZ)(\rho,\phi,Z_*)$. Now, however, (64) is not applicable. Instead, we now fix (cf. the first equation in (62))

[2] We regret an error in the definition of v^- in Ref. [6], Eq. (42). The correct expressions are $v^\pm = [T'_0(\pm1), T'_1(\pm1), T'_2(\pm1), T'_3(\pm1), T'_4(\pm1), \cdots] = [0, 1, \pm4, 9, \pm16, \cdots]$. In Ref. [6] the right-hand side of the second equation of (69) is also off by a sign.

$$\sum_{k=0}^{N_Z^1} \widetilde{\psi}^1_{qnk}\delta^+_k = \tilde{f}^+_{qn}, \quad \tilde{e}^-_{qn} = \sum_{k=0}^{N_Z^2} \widetilde{\psi}^2_{qnk}\alpha_2 v^-_k, \tag{65}$$

where here $\tilde{f}^+_{qn}$ (for $0 \leqslant q \leqslant N^1_\phi$ and $0 \leqslant n \leqslant N^1_\rho$) and $\tilde{e}^-_{qn}$ (for $0 \leqslant q \leqslant N^2_\phi$ and $0 \leqslant n \leqslant N^2_\rho$) are not to be viewed as inhomogeneities, rather as expressions built respectively with the modal coefficients for $\mathcal{P}\psi^2(\rho,\phi,Z_*)$ and $(d\mathcal{P}\psi^1/dZ)(\rho,\phi,Z_*)$. Note that, as with Eq. (64), these equations have the form "cylinder 1 coefficients = cylinder 2 coefficients".

Let us consider only $\tilde{f}^+_{qn}$, since similar comments apply to $\tilde{e}^-_{qn}$. First, we start with cylinder 1 and define a Chebyshev–Lobatto/Fourier grid $\{(\rho_j,\phi_i) : 0 \leqslant j \leqslant N^1_\rho,\ 0 \leqslant i \leqslant N^1_\phi\}$ on the $Z = Z_*$ cap of cylinder 1. The use of these points affords a double discrete Fourier–Chebyshev transform, through numerical quadrature, relating function values at the points and mode coefficients. (In practice, we have exploited the trigonometric form of the Chebyshev polynomials and have used the FFT to define both the Fourier and Chebyshev components of this transform.) The double discrete transform allows us to express the modal coefficients $\tilde{f}^+_{qn}$ in terms of the function values f^+_{ij}, at (ρ_i,ϕ_j), for $Z = Z_*$ on cylinder 1, in a form

$$\tilde{f}^+_{qn} = \sum_{i=0}^{N^1_\rho}\sum_{j=0}^{N^1_\phi} \mathcal{F}_{qn,ij} f^+_{ij}. \tag{66}$$

Next, at the nodal points (ρ_j,ϕ_i) of cylinder 1, we evaluate f^+_{ij} in terms of the expansion for the solution on cylinder 2, thereby finding

$$f^+_{ij} = \mathcal{P}\psi^2(\rho_j,\phi_i,Z_*) = \sum_{q=0}^{N^2_\phi}\sum_{n=0}^{N^2_\rho} \mathcal{E}_{ij,qn} \sum_{k=0}^{N^2_Z} \widetilde{\psi}^2_{qnk}\delta^-_k. \tag{67}$$

Here, the values $\mathcal{E}_{ij,qn}$ arise from the evaluations of the modal functions (Chebyshev and Fourier) of cylinder 2 at the nodal points (ρ_j,ϕ_i) of cylinder 1. When the expressions for f^+_{ij} from (67) are substituted in (66), we get expressions for $\tilde{f}^+_{qn}$ in terms of the modal coefficients $\widetilde{\psi}^2_{qnk}$ representing the solution in cylinder 2. Finally, we substitute this $\tilde{f}^+_{qn}$ into (65), which yields relationships between the modal coefficients on cylinder 1 and cylinder 2 that express continuity of the solution across $Z = Z_*$.

The linear relationships (65) would likewise be inserted into the overall coefficient matrix $\mathcal{M}$. Similar to before, the right-hand side of the first equation in (65) would fill empty rows stretching across the 1–2 super-block, with the δ^+ vectors on the left-hand side filling empty rows across the 1–1 super-block. The relationships expressed in the second equation in (65) would fill empty rows stretching across the 2–2 and 2–1 super-blocks Finally, we note that the Eq. (65) reduce to (64) when $N^1_\phi = N^2_\phi$ and $N^1_\rho = N^2_\rho$.

3.2. Gluing of an inner shell to cylinders and blocks

The shells J and H in Fig. 1 overlap multiple blocks and cylinders. We focus on gluing H to the combination of blocks C, D and cylinders 3, 4, 5. Let $\mathcal{S}$ represent one of $C, D, 3, 4, 5$, and consider the portion $\partial H^+_{\mathcal{S}}$ of ∂H^+ which intersects subdomain $\mathcal{S}$. At nodal points on $\partial H^+_{\mathcal{S}}$ we require that the values of ψ agree whether they are computed with $\widetilde{\boldsymbol{\psi}}^H$ or $\widetilde{\boldsymbol{\psi}}^{\mathcal{S}}$. For nodal points $(\theta_j,\phi_k) \in \partial H^+_{\mathcal{S}}$ this condition is (cf. Eq. (45))

$$h^+_{jk} \equiv h^+(\theta_j,\phi_k) = \mathcal{P}\psi^{\mathcal{S}}(\mathbf{x}(r_{\max},\theta_k,\phi_j)). \tag{68}$$

Here $\mathcal{P}\psi^{\mathcal{S}}$ is the numerical solution ($\mathcal{P}$ indicates finite expansion) associated with $\widetilde{\boldsymbol{\psi}}^{\mathcal{S}}$, and $\mathbf{x}$ are the relevant 3D coordinates on subdomain $\mathcal{S}$. Looping over $\mathcal{S} = C, D, 3, 4, 5$ defines the grid function h^+_{jk} at all nodal points of ∂H^+. The matching conditions (+ case in (45)) can then be realized by expressing the spherical harmonic transform $\tilde{h}^+_{\ell q} = \sum_{j=0}^{N_\theta}\sum_{k=0}^{2N_\theta} \mathcal{Q}_{\ell q,jk} h^+_{jk}$ as a matrix–vector product involving *all* $\widetilde{\boldsymbol{\psi}}^{\mathcal{S}}$. The resulting equations are placed in empty rows of $\mathcal{M}$ which stretch across the *H-H* and *all H-*$\mathcal{S}$ super-blocks.

Again let $\mathcal{S}$ represent one of $C, D, 3, 4, 5$. Then $\partial\mathcal{S}$ includes a portion $\partial\mathcal{S}_H$ overlapping shell H which gives rise to further gluing relations. These equations will be inserted into empty rows of $\mathcal{M}$ which stretch across the $\mathcal{S}$-$\mathcal{S}$ and $\mathcal{S}$-H super-blocks. For concreteness, take $\mathcal{S} = C$, and so the + case in (10). Now $\tilde{h}^+_{nm}$ is the double *XY*-Chebyshev transform of

$$h^+_{jk} = \sum_{n=0}^{N_r}\sum_{\ell=0}^{N_\theta} \widetilde{\psi}^H_{\ell 0 n}\overline{P}_{\ell 0}(\cos\theta_{jk}) T_n(\xi(r_{jk})) + \sum_{n=0}^{N_r}\sum_{\ell=1}^{N_\theta}\sum_{m=1}^{N_\theta} \overline{P}_{\ell m}(\cos\theta_{jk}) \left[\widetilde{\psi}^H_{\ell,2m-1,n}\cos(m\phi_{jk}) + \widetilde{\psi}^H_{\ell,2m,n}\sin(m\phi_{jk})\right] T_n(\xi(r_{jk})). \tag{69}$$

Here $(r_{jk},\theta_{jk},\phi_{jk}) \in H$ is also a Chebyshev–Gauss–Lobatto node $(X(\xi_j), Y(\eta_k), Z_{\max})$ on the top *XY*-face of C. The matrix representation $\tilde{h}^+_{nm} = \sum_{j=0}^{N_X}\sum_{k=0}^{N_Y} \mathcal{F}_{nm,jk} h^+_{jk}$ of the transform then yields equations between $\widetilde{\boldsymbol{\psi}}^C$ and $\widetilde{\boldsymbol{\psi}}^H$. As mentioned, these equations then fill empty rows of $\mathcal{M}$ which stretch across the *C-C* and *C-H* super-blocks.

3.3. Gluing of a cylinder to a block

Here we sketch either the gluing of block B and cylinder 1, block C and cylinder 3, or block D and cylinder 5. We focus on the middle case as a representative example. This process involves both (a) gluing two *YZ* and two *XZ* faces of block C to cylinder 3, and (b) gluing the inner radial boundary of the cylinder to the block. The process for (a) is similar to the gluing

described in the last paragraph (in which a face of C is glued to H), and we omit a description. To express the matching equations which enforce (b), we first define

$$q^-_{jk} = \sum_{n=0}^{N_X}\sum_{m=0}^{N_Y}\sum_{p=0}^{N_Z} \widetilde{\psi}^C_{nmp} T_n(\xi(X_{jk}))T_m(\eta(Y_{jk}))T_p(\chi(Z_{jk})). \tag{70}$$

Here we use the following points:

$$(X_{jk}, Y_{jk}, Z_{jk}) = \big(X(\rho_{\min}, \phi_j, z_k), Y(\rho_{\min}, \phi_j, z_k), Z(\rho_{\min}, \phi_j, z_k)\big), \tag{71}$$

where $(\rho_{\min}, \phi_j, z_k)$ are nodal points along the inner radial boundary of cylinder 3. Next, we consider the Fourier–Chebyshev transform $\tilde{q}^-_{mp} = \sum_{j=0}^{N_\phi}\sum_{k=0}^{N_z} \mathcal{C}_{mp,jk} q^-_{jk}$. In terms of the transform the matching equations are

$$\sum_{n=0}^{N_\rho} \widetilde{\psi}^3_{mnp}\delta^-_n = \tilde{q}^-_{mp}. \tag{72}$$

These equations then fill empty rows of $\mathcal{M}$ which stretch across the 3–3 and 3-C superblocks.

4. Numerical solution of the 3d HRWE

Both on single subdomains and on the global 2-center multidomain $\mathcal{D}$, this section considers numerical solution of the HRWE for the field of two point sources in a circular binary orbit. For this problem we have essentially an exact solution, a superposition of the fields for two point sources, each point source in a circular orbit and described by the Liénard–Wiechert solution (A.9) found in the appendix. A numerical solution is a collection of modal expansion coefficients; however, comparisons with the exact solution are always computed in physical space on the nodal grid (or grids in the multidomain case) dual to the modal expansion. These nodal grids are coarse, and the norms reported in the tables do not settle down quickly. All numerical solves are performed iteratively with preconditioned GMRES [33], and this section also describes the relevant preconditioning (both for subdomain solves and for the global multidomain solve). Table 4 lists the parameters used in all computations and describes their relationship with the coordinate systems introduced in Section 1.2.

Using the sparse representations described in Section 2, in Section 4.1 we numerically solve the HRWE on the following subdomains (cf. Fig. 2 and Table 4): the outer shell O, (inner) spherical shell J, (inner) cylindrical shell 5, and (inner) block D. For each subdomain labeled (inner) the HRWE operator is implemented as a matrix–vector multiply within preconditioned GMRES without restarts. For these subdomain solves, Dirichlet boundary conditions are taken from the exact Liénard–Wiechert solution, but the outer shell problem also involves the radiation boundary conditions given in Eq. (22). The particular subdomains considered in Section 4.1 are representative, and similar experimentation on each subdomain has determined the chosen truncations for the 2-center multidomain tests described in Section 4.2. Such experiments empirically yield appropriate truncations necessary to achieve a desired accuracy. All tests in Sections 4.1 and 4.2 involve two charges, one with $z_H = 1, Q_H = 1$ and the other with $z_J = -0.9,\ Q_J = 0.5$. Section 4.1 considers $\Omega = 0.1, 0.3$. We have also considered $\Omega = 0.5, 0.7$ (chosen to "break" our methods) [38], but give no results here.

4.1. Numerical solution on individual subdomains

We consider the outer shell O first, since results for this subdomain are the most disappointing. The solve for O differs from the rest. Indeed, since the representation of the HRWE on O is comprised of blocks labeled by (ℓ, m) along the block diagonal, we invert each of these physical modes using LU-factorization [the "physical mode-blocks using" are those *not* annihilated by the projection operator $\mathbb{P}$ defined in (14)]. Let $N_\theta = \ell_{\max}$, so that $\mathcal{N} = (N_\theta + 1)(2N_\theta + 1)(N_r + 1)$ is the system size, with $\mathcal{N}^2 \sim 4N_\theta^4 N_r^2$ the storage requirement for the full coefficient matrix. However, storage of all blocks involves $(N_\theta + 1)$ matrices of size $(N_r + 1)$-by-$(N_r + 1)$, one for each zero mode, in addition to $\frac{1}{2}N_\theta(N_\theta + 1)$ matrices of size $2(N_r + 1)$-by-$2(N_r + 1)$, one for each fixed-m cos/sin pair. Therefore, storage for this solve scales like

Table 4
Domain decomposition. J and H are respectively centered at $(\widetilde{X}, \widetilde{Y}, \widetilde{Z}) = (0, 0, -0.9)$ and $(0, 0, 1.0)$; for each the polar system $\{r, \theta, \phi\}$ is relative to the Cartesian system arising from translation of $\{\widetilde{X}, \widetilde{Y}, \widetilde{Z}\}$ to the shell's origin. For each cylinder, $\{\rho, \phi, \widetilde{Z}\}$ are cylindrical coordinates relative to $\{\widetilde{X}, \widetilde{Y}, \widetilde{Z}\}$. The spherical polar coordinates $\{r, \theta, \varphi\}$ for O are relative to $\{\widetilde{x}, \widetilde{y}, \widetilde{z}\}$.

Spherical shells (all with $0 \leqslant \theta \leqslant \pi$; $0 \leqslant \phi < 2\pi$ for J and H; $0 \leqslant \varphi < 2\pi$ for O)				
$J : 0.4 \leqslant r \leqslant 1.1$;	$H : 0.3 \leqslant r \leqslant 1.1$;	$O : 2.0 \leqslant r \leqslant 150.0$		
Cylindrical shells (all with $0.452 \leqslant \rho \leqslant 2.120$ and $0 \leqslant \phi < 2\pi$)				
$1 : -2.120 \leqslant \widetilde{Z} \leqslant -1.525$;	$2 : -1.525 \leqslant \widetilde{Z} \leqslant -0.275$;	$3 : -0.275 \leqslant \widetilde{Z} \leqslant 0.375$;	$4 : 0.375 \leqslant \widetilde{Z} \leqslant 1.625$;	$5 : 1.625 \leqslant \widetilde{Z} \leqslant 2.120$
Blocks (all with $-0.640 \leqslant \widetilde{X}, \widetilde{Y} \leqslant 0.640$)				
$B : -2.120 \leqslant \widetilde{Z} \leqslant -1.525$;	$C : -0.275 \leqslant \widetilde{Z} \leqslant 0.375$;	$D : 1.625 \leqslant \widetilde{Z} \leqslant 2.120$		

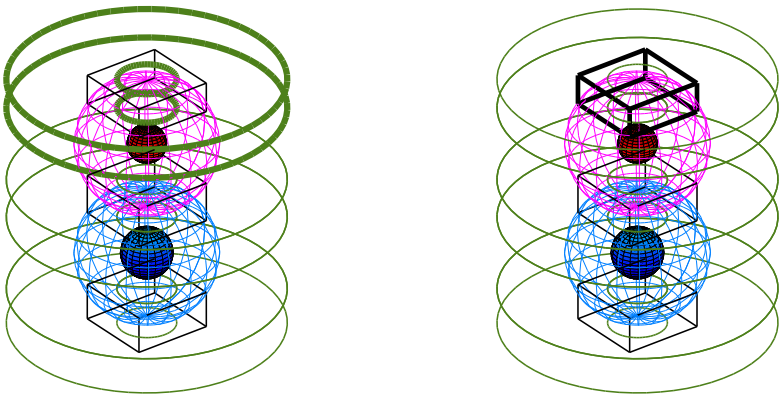

(a) Cylinder experiment. (b) Block experiment.

Fig. 2. Individual subdomains. We consider cylindrical shell five highlighted in the left figure, block D highlighted in the right, and the bottom inner spherical shell J shown in both.

Table 5
Outer spherical shell O test.

N_r	$\ell_{\max}$	L_2 error	L_2 norm	L_∞ error	L_∞ norm
$\Omega = 0.1$					
65	10	1.1899E-05	1.8977E-01	2.7970E-04	1.1808E+00
85	18	2.1320E-07	1.8725E-01	3.6548E-06	1.1810E+00
125	28	2.4580E-10	1.8472E-01	5.4193E-09	1.1810E+00
185	42	2.2846E-13	1.8297E-01	2.7858E-12	1.1810E+00
$\Omega = 0.3$					
65	10	7.4142E-04	1.9030E-01	1.0557E-02	1.2624E+00
85	18	9.4481E-04	1.8777E-01	1.3180E-02	1.2628E+00
125	28	1.2701E-04	1.8523E-01	2.0861E-03	1.2628E+00
185	42	5.1221E-06	1.8347E-01	1.2307E-04	1.2628E+00

$$(N_\theta + 1)(N_r + 1)^2 + 2N_\theta(N_\theta + 1)(N_r + 1)^2 \sim 2N_\theta^2 N_r^2 = O(N_r \cdot \mathcal{N}). \tag{73}$$

As shown in Table 5, the results for $\Omega = 0.1$ are excellent, but degradation has already set in for $\Omega = 0.3$ (for large Ω multiple concentric outer shells may yield more accuracy).

We next consider the inner spherical shell J. Tables 6 and 7 list errors, without and with preconditioning. For the sake of comparison, in both these and subsequent tables we have chosen the same requested tolerances (for the GMRES solve) for both values of Ω. The chosen preconditioner is block-Jacobi. Namely, we invert physical mode-blocks labeled by (ℓ, m) along the block diagonal using a precomputed LU-factorization. The storage and scaling properties for this preconditioner are exactly the same as described for the direct solve on the outer shell. However, for inner shells the HRWE representation is not block diagonal in (ℓ, m) pairs (as on the outer shell), rather the operator has significant bandwidth in both indices. Therefore, the full matrix storage for an inner shell would require correspondingly larger memory relative to the preconditioner storage. Further, the preconditioner storage requirement could be reduced by inverting each sin/cos block mode independently.

Table 6
Inner spherical shell test J without preconditioning.

N_r	$\ell_{\max}$	L_2 error	L_2 norm	L_∞ error	L_∞ norm	Iterations	Tolerance
$\Omega = 0.1$							
12	12	3.4702E-06	1.3516E+00	2.2656E-05	1.9143E+00	54	1.0000E-07
18	23	9.9814E-09	1.3499E+00	3.6488E-08	1.9168E+00	129	1.0000E-09
20	33	6.0107E-11	1.3498E+00	2.6944E-10	1.9173E+00	238	1.0000E-11
30	46	6.2864E-13	1.3481E+00	2.8333E-12	1.9176E+00	415	1.0000E-13
$\Omega = 0.3$							
12	12	7.6593E-06	1.3566E+00	7.8541E-05	1.9255E+00	57	1.0000E-07
18	23	2.1272E-08	1.3550E+00	3.8188E-07	1.9278E+00	138	1.0000E-09
20	33	1.1806E-10	1.3550E+00	2.4707E-09	1.9283E+00	255	1.0000E-11
30	46	4.3184E-13	1.3532E+00	5.2289E-12	1.9286E+00	442	1.0000E-13

Table 7
Inner spherical shell J test with preconditioning.

N_r	ℓ_{max}	L_2 error	L_2 norm	L_∞ error	L_∞ norm	Iterations	Tolerance
$\Omega = 0.1$							
12	12	3.4196E-06	1.3516E+00	2.2499E-05	1.9143E+00	3	1.0000E-07
18	23	3.4877E-09	1.3499E+00	3.6560E-08	1.9168E+00	4	1.0000E-09
20	33	1.3949E-11	1.3498E+00	2.1394E-10	1.9173E+00	4	1.0000E-11
30	46	3.0104E-14	1.3481E+00	3.0975E-13	1.9176E+00	5	1.0000E-13
$\Omega = 0.3$							
12	12	7.6487E-06	1.3566E+00	7.8536E-05	1.9255E+00	4	1.0000E-07
18	23	2.0798E-08	1.3550E+00	3.8215E-07	1.9278E+00	6	1.0000E-09
20	33	1.0362E-10	1.3550E+00	2.4686E-09	1.9283E+00	7	1.0000E-11
30	46	1.0361E-13	1.3532E+00	3.1604E-12	1.9286E+00	9	1.0000E-13

Table 8
Cylindrical shell five test with preconditioning.

N_r	N_ϕ	N_z	L_2 error	L_2 norm	L_∞ error	L_∞ norm	Iterations	Tolerance
$\Omega = 0.1$								
13	5	7	7.9884E-08	9.0116E-01	4.6388E-07	1.5004E+00	3	1.0000E-08
19	9	9	5.2802E-10	8.9887E-01	2.7463E-09	1.5006E+00	4	1.0000E-10
23	13	13	5.6239E-13	8.9775E-01	4.4170E-12	1.5006E+00	5	1.0000E-12
29	19	18	8.3992E-15	8.9680E-01	9.3259E-14	1.5007E+00	6	1.0000E-14
$\Omega = 0.3$								
13	5	7	6.2980E-06	9.4046E-01	3.8531E-05	1.5817E+00	6	1.0000E-08
19	9	9	1.2577E-07	9.3796E-01	5.9139E-07	1.5841E+00	10	1.0000E-10
23	13	13	4.9307E-09	9.3677E-01	4.0773E-08	1.5849E+00	14	1.0000E-12
29	19	18	3.2422E-10	9.3574E-01	1.3965E-09	1.5861E+00	18	1.0000E-14

Moreover, were the preconditioner chosen to correspond to only the Laplacian part of the operator, then it could be used for the solves on both shells were their dimensions and truncations the same. In any case, the chosen preconditioner notably improves the convergence of the GMRES solver.

Table 8 list the results for the corresponding single cylinder experiment, with block *LU*–preconditioning similar to before. That is, for each Fourier mode we invert the associated diagonal block. Our choice (50) of direct product structure for the cylinders determines that each block is $(N_\rho+1)(N_Z+1)$-by-$(N_\rho+1)(N_Z+1)$. For cylinders, preconditioning amounts to direct inversion of each Fourier mode-block along the block diagonal. With $\mathcal{N} = (N_\phi+1)(N_\rho+1)(N_z+1)$ the system size, the storage requirement for the preconditioner requires $N_\phi+1$ matrices of size $(N_\rho+1)(N_z+1)$-by-$(N_\rho+1)(N_z+1)$, and so scales like so

$$(N_\rho+1)^2(N_z+1)^2(N_\phi+1) = O(N_\rho N_z\cdot\mathcal{N}). \tag{74}$$

While $N_\rho N_z\mathcal{N} < \mathcal{N}^2$, this requirement is somewhat memory intensive. However, we have observed essentially the same performance when using the corresponding Laplacian part of the operator to define the preconditioner. Provided that the dimensions and truncations of two individual cylinders match, the same preconditioner could then be used for both.

Table 9 list errors for the block experiment, and again with a block-Jacobi preconditioner. In this case there are N_x+1 blocks with size $(N_y+1)(N_z+1)$-by-$(N_y+1)(N_z+1)$. Storage of the block preconditioner therefore scales as

$$(N_x+1)(N_y+1)^2(N_z+1)^2 = O(N_y N_z\cdot\mathcal{N}). \tag{75}$$

Again, were the preconditioner based on the Laplacian part of the operator, it might be reused for the solves on different blocks.

4.2. Numerical solution on the 2-center multidomain

We have also used GMRES [33] to solve the linear system $\mathcal{M}\widetilde{\mathbf{\Psi}} = \mathcal{B}\widetilde{\mathcal{G}}$ given in Eq. (63) for the HRWE on the whole 2-center domain $\mathcal{D}$. Sections 2 and 3 have described the matrix $\mathcal{M}$, and therefore also implementation of the "matrix–vector multiply" $\widetilde{\mathbf{\Psi}} \to \mathcal{M}\widetilde{\mathbf{\Psi}}$. Implementation of this multiply is required by the GMRES algorithm (with or without preconditioning). However, an *unpreconditioned* GMRES strategy results in extremely poor convergence. Therefore, we have used (left) *preconditioned* GMRES which further requires implementation of the operation $\widetilde{\mathbf{\Psi}} \to \mathcal{M}^{-1}_{approx}\widetilde{\mathbf{\Psi}}$, where $\mathcal{M}^{-1}_{approx} \simeq \mathcal{M}^{-1}$ is an approximate inverse. In this section we describe application of $\mathcal{M}^{-1}_{approx}$, and document tests of the global solve. We stress that the preconditioning afforded by $\mathcal{M}^{-1}_{approx}$ is neither (i) the integration "preconditioning" technique used to achieve sparse representations of (4) on each of the basic subdomains nor (ii) the preconditioning (typically a form of block-*LU*) used for individual subdomain solves. However, type (ii) preconditioning does define part of the $\mathcal{M}^{-1}_{approx}$ application.

Table 9
Block D test with preconditioning.

N_x	N_y	N_z	L_2 error	L_2 norm	L_∞ error	L_∞ norm	Iterations	Tolerance
$\Omega = 0.1$								
14	14	7	3.7513E-07	1.1367E+00	4.2360E-06	1.7854E+00	41	1.0000E-08
19	19	9	6.3235E-09	1.1394E+00	1.3616E-07	1.8098E+00	62	1.0000E-10
28	28	13	1.4351E-11	1.1418E+00	3.0822E-10	1.8040E+00	102	1.0000E-12
32	32	18	1.2749E-13	1.1421E+00	5.3182E-12	1.8054E+00	141	1.0000E-14
$\Omega = 0.3$								
14	14	7	3.9020E-07	1.1955E+00	4.2789E-06	1.8911E+00	42	1.0000E-08
19	19	9	6.4495E-09	1.1986E+00	1.4194E-07	1.9176E+00	65	1.0000E-10
28	28	13	1.4448E-11	1.2013E+00	4.9319E-10	1.9116E+00	109	1.0000E-12
32	32	18	8.4807E-14	1.2017E+00	2.9017E-12	1.9131E+00	154	1.0000E-14

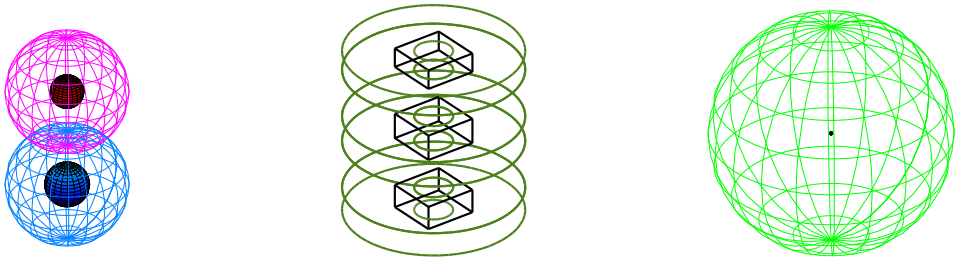

(a) Inner shells J and H. (b) Glued subregion R. (c) Outer shell O.

Fig. 3. Alternating schwarz preconditioner. Numerical solution of the HRWE each subdomain/subregion above defines the preconditioner. Boundary conditions for the solves are obtained through subdomain/subregion interpolation as described in the text. For the outer shell shown in (c), the small dot in the center is, to scale, the inner configuration comprised of (a) and (b).

The action of $\mathcal{M}^{-1}_{approx}$ is defined through the simple alternating Schwarz method [39]. Application of this preconditioner relies on independent numerical solves over (i) the inner shells J and H, (ii) the glued subregion[3] R comprised of blocks and cylinders depicted in Fig. 3, and (iii) the outer spherical shell O. More precisely, starting with a vanishing initial vector $\widetilde{\mathbf{\Psi}}$ we perform the following iteration.

1. Solve (also by GMRES, as described in Section 4.1) the HRWE on the inner shells J and H. For these solves inner Dirichlet boundary conditions are the fixed physical ones, while outer boundary conditions stem from interpolation of the numerical solution on R (which is initially zero). The tolerance for these solves is typically `0.1*tol`, where `tol` is the tolerance for the global GMRES solve of $\mathcal{M}\widetilde{\mathbf{\Psi}} = \mathcal{B}\widetilde{\mathcal{G}}$.
2. Solve (also by GMRES) the HRWE on R. For this solve inner Dirichlet boundary conditions stem from interpolation of the solutions on J and H, while outer Dirichlet boundary conditions stem from interpolation of the solution on the outer shell O (which is initially zero). This GMRES solve must also be preconditioned, as discussed shortly. The tolerance for this solve is typically `0.2*tol`.
3. Solve the HRWE on the outer spherical shell O, with inner Dirichlet boundary conditions stemming from interpolation of the numerical solution on R and the outer radiation boundary conditions described in Section 2.1. As noted in Section 4.1, this solve is performed via direct block-by-block LU factorization (note that the factorization of each block mode is *precomputed* and then used over and over in this third step).

This three-step iteration may be viewed as the Gauss–Seidel method, here applied in block form to $J \bigcup H, R, O$. Typically, we have chosen four sweeps of this block Gauss–Seidel method. Step 2 requires its own preconditioning to enhance convergence. Here we have again employed the alternating Schwarz method, now with blocks corresponding to B, C, D, and the subregion G which is the composite of glued cylinders (1–5). This "inner" preconditioning typically involves five sweeps, with appropriate interpolation. Each individual GMRES solve on B, C, D, and G uses the tolerance `0.1*tol`. Table 10 depicts the overall scheme.

Before turning to tests of the full solve, we consider the solve on the multidomain subregion G comprised of the glued cylinders (1–5). Again, this solve is performed as part of the preconditioner for step 2 of the global preconditioner (see Table 10).

[3] Whereas the basic spectral elements (such as shell J, block B, and cylinder 1) have been called *subdomains*, we informally refer to the multidomains R and G (defined later) as *subregions*.

Table 10
Multilevel preconditioning scheme.

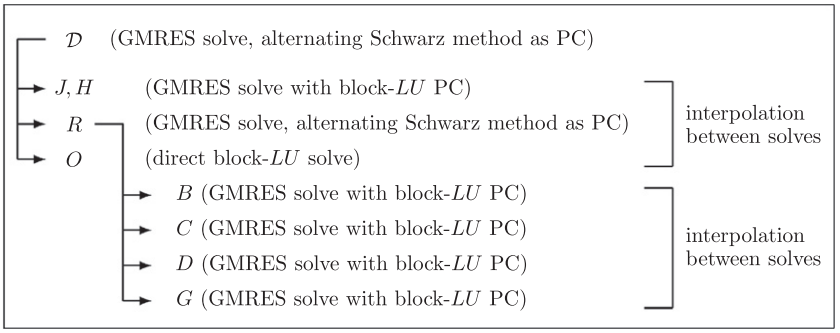

Table 11
Solution of the HRWE on the glued cylinder subregion G. The reported truncations N_r^1 and N_ϕ^1 were also used for cylinders 2, 3, 4, and 5.

N_r^1	N_ϕ^1	N_z^1	N_z^2	N_z^3	N_z^4	N_z^5	L_2 error	L_2 norm	L_∞ error	L_∞ norm	Iterations	Tolerance
$\Omega = 0.1$												
13	5	7	17	7	17	7	2.2251E-06	9.8806E-01	2.7804E-05	2.4773E+00	17	1.0000E-06
19	9	9	23	9	23	9	3.5812E-08	1.0077E+00	2.2023E-07	2.4781E+00	22	1.0000E-08
23	13	14	31	16	31	14	1.2344E-10	1.0063E+00	1.2046E-09	2.4782E+00	28	1.0000E-10
29	19	15	35	15	35	15	6.6478E-12	1.0083E+00	7.4462E-11	2.4783E+00	42	1.0000E-12
29	19	18	39	21	39	18	4.9252E-13	1.0063E+00	5.3570E-12	2.4783E+00	45	1.0000E-13

Table 12
Solution of the HRWE on the 2-center multidomain $\mathcal{D}$. Here MPSPD stands for *modes per subdomain per dimension*. Note that an MPSPD of 37.9 corresponds to (11 subdomains) $\times$ (37.9^3) $\simeq$ 599000 unknowns.

MPSPD	L_2 error	L_2 norm	L_∞ error	L_∞ norm	Iterations	Tolerance
$\Omega = 0.1$						
15.7	3.7532E-06	7.0509E-01	9.9579E-05	3.6556E+00	5	1.0000E-05
23.9	4.2440E-08	7.8382E-01	5.8222E-07	3.6563E+00	3	1.0000E-07
31.0	2.6333E-10	8.3492E-01	4.0406E-09	3.6564E+00	3	1.0000E-09
37.2	4.1855E-12	9.3982E-01	8.6696E-11	3.6565E+00	3	1.0000E-11
37.9	4.7733E-13	9.5252E-01	8.2254E-12	3.6565E+00	2	1.0000E-12

Table 11 collects errors and iteration counts associated with this solve for increasing truncations. Each solve documented in the table has been started with the zero vector as initial iterate, and here we employ restarting after 20 iterations. The reported iteration counts in Table 11 are cumulative over restarts. The individual block-*LU* preconditioning on each subdomain (1–5) is the only preconditioning used for this solve. Nevertheless, it suffices to drastically reduce the number of iterations (which would otherwise be in the thousands, with or without restarts).

Results for the full solve appear in Table 12. The largest solve involves more than half a million unknowns (597788 to be precise). In fact the number of unknowns is larger, since we add modes to shells, but here count only physical (ℓ, m) pairs (cf. Section 2.1). Each solve in the table is used as the initial guess for the next, and the iteration count therefore drops.

5. Conclusion

We close by summarizing our results and describing future work. In our summary and description, we discuss our numerical methods and the physical problem we aim to solve.

5.1. Results

We have demonstrated the feasibility of solving a partial differential equation in three independent variables by modal spectral methods based on the technique of integration preconditioning. As designed, the technique yields an algorithmic

way to achieve a sparse spectral formulation of the PDE problem with consistent incorporation of boundary conditions. However, particularly in higher dimensional settings, an integration "preconditioner" may not be an optimal approximate inverse in any known sense; as a result the technique would not seem practical in and of itself. Here we mean that, for a higher dimensional problem like ours, the sole use of integration preconditioning will likely lead to prohibitively large iteration counts when using Krylov methods and/or loss of accuracy due to poor conditioning. At least for our problem, we have demonstrated that both issues may be surmounted by *further preconditioning*. In particular, studying our problem on a given subdomain (spectral element), we have empirically demonstrated that block Jacobi preconditioning (with each block inverted by *LU* factorization) is effective for the banded matrix produced by integration preconditioning. Moreover, for the matching of subdomains in our multidomain approach the alternating Schwarz method (an elementary domain decomposition preconditioner) works well. Given that little seems known about preconditioning for modal methods, whereas preconditioning for nodal methods is well developed, we believe that our demonstration of effective modal preconditioning based on rather standard methods is remarkable.

In addition to modal preconditioning, other aspects of our work are new from the standpoint of modal spectral methods, in particular its multidomain character and focus on a mixed-type problem. Ref. [1] already presented the outline for applying the integration preconditioning technique to higher dimensional problems, that is to PDEs. While we have carried out and presented the details of such an application, our work has gone further in developing a 3D *multidomain* version of the technique (Ref. [6] consider the multidomain case in 2D). In particular, we have presented the details of gluing constituent subdomains, and how this gluing is reflected in the overall linear system. As another new, and unusual, aspect, our work is the first successful application of integration preconditioning to a three dimensional mixed-type problem, a problem with both elliptic and hyperbolic regions. Whence it has numerically confirmed once more (cf. [6,26,27,29]) that such problems can be well-posed; see [43] for a theoretical discussion. A multidomain decomposition is of special interest for mixed problems like ours, since the type change need not occur in all subdomains. For our example, it occurs on a cylinder that intersects only the outer spherical shell. When the nonlinearities of the physical problem are included, this feature of our domain decomposition may prove useful, because the true physical equations will be only mildly nonlinear on the outer shell, with the strongest nonlinearities confined to subdomains on which the equations are elliptic. Our work therefore suggests that we might treat the outer shell differently from the inner subdomains when solving the full nonlinear problem.

5.2. Outlook

While we have shown that our mix of methods delivers efficiency and remarkable accuracy when applied to a nontrivial 3D model problem, several issues merit further investigation. These include both particular challenges in the application of this paper's methods to helically symmetric general relativistic binary fields (our problem of interest), and numerical analysis questions pertaining to integration preconditioning for more general problems.

The numerical analysis issues center on the value of integration preconditioning, or sparsification, in the solution of higher dimensional PDEs, particularly in the context of a multidomain approach. Here we have applied the method to only one linear PDE, with an empirical demonstration of its success. For any given linear equation, a fuller investigation of integration sparsification for multidomain scenarios would focus on the interplay between condition number, field of values (Rayleigh quotients), and computational efficiency (iteration counts). All of these issues would be examined both before and after some form of "ordinary" preconditioning, e.g. the combination of block-*LU* and alternating Schwarz preconditioning used in this paper. The sparse matrices produced by integration sparsification allow for fast matrix multiplies in a Krylov method like GMRES. Our work suggests that this advantage might be gained without large iteration counts, but the issue deserves more study. Efficient treatment of nonlinearities is also worthy of investigation, and such a study would build upon the results already given in Ref. [1]. We are in process of evaluating integration sparsification in the context of these issues, mostly with 2D model problems.

Several challenges remain if we are to apply some variant of our method to the problem of helically symmetric general relativistic binary fields. First, we must test the efficiency of our method in solving a nonlinear HRWE. In practice, this should not be a problem. The strongest nonlinearities will occur closest to the black hole sources, i.e. near the surfaces on which the inner boundary conditions are set. By choosing these boundaries some distance from the sources, we can, at the cost of accuracy in mathematically representing the physical problem, reduce the severity of the nonlinearities. The real question, then, is not whether we can handle nonlinearities, but how close to the sources the inner boundaries can be placed. Second, we must replace the outgoing radiative boundary conditions with "standing wave boundary conditions," as described in Ref. [25]. This change is straightforward in a linearized problem, and, as explained in Ref. [25], should not pose great difficulty in nonlinear general relativity. Third, we must move from the scalar problem considered here to the actual tensor problem. Solution of the helically symmetric problem of a binary in full general relativity will require all the information in the tensorial fields, and the coupling of those fields. This proved to be the greatest challenge for the solution method presented in Ref. [29], and it severely limited the achievable accuracy. We are confident that the method described in this paper will deliver the accuracy needed to find useful solutions.

The methods developed here have been motivated by the problem of binary inspiral in general relativity. However, our methods may find broader use; they might be applied to problems distinct from the helically symmetric mixed PDEs of the periodic standing wave approximation. As a salient example, multidomain spectral methods are already being used in the

elliptical problem of generating binary black hole initial data [30,31]. Our set of methods, with integration sparsification, might be used as an alternative approach.

Acknowledgments

We gratefully acknowledge support from NSF Grant PHY 0855678 to the University of New Mexico. For helpful comments and discussions we thank T. Hagstrom, J. Hesthaven, H. Pfeiffer, G. von Winckel, and particularly E. Coutsias. We also thank both the developers of the GMRES routines described in [33], and those of Spherepack 3.0 [40].

Appendix A. Explicit solution for a point source

This appendix considers the wave equation forced by a point source in a circular orbit (see Ref. [41] for the analogous electrodynamics problem), thereby constructing a solution to the HRWE. Superposition of two such solutions yields the binary field used in our numerical tests. We derive two representations for the solution. Using both representations, we can evaluate the binary field with enough accuracy (uniformly over the 2-center domain $\mathcal{D}$) to make the comparisons reported in Section 4. Precisely, we seek the *retarded* solution to

$$\left(\nabla^2 - \partial_t^2\right)\Psi = -4\pi\delta^{(3)}(\mathbf{x} - \boldsymbol{\xi}(t)), \tag{A.1}$$

where the *subluminal* motion of source point is

$$\boldsymbol{\xi}(t) = a\cos(\Omega t)\mathbf{e}_x + a\sin(\Omega t)\mathbf{e}_y, \quad a\Omega < 1. \tag{A.2}$$

To find a series solution, we assume $\Psi(t,x,y,z) = \psi(\tilde{x},\tilde{y},z)$ in terms of the comoving coordinates (1). This assumption transforms (A.1, A.2) into the inhomogeneous HRWE

$$\left(\tilde{\nabla}^2 - \Omega^2\partial_\varphi^2\right)\psi = -4\pi\frac{\delta(r-a)}{a^2}\delta(\cos\theta)\delta(\varphi), \tag{A.3}$$

where $\tilde{\nabla}^2 \equiv \partial_{\tilde{x}}^2 + \partial_{\tilde{y}}^2 + \partial_z^2$ and $(a,\pi/2,0)$ specifies the location of the source point in the spherical polar system associated with $(\tilde{x},\tilde{y},z)$. Using standard methods of separation of variables and one-dimensional Green's functions, and assuming the outgoing boundary conditions, we find a particular solution to (A.3),

$$\begin{aligned}\psi(r\sin\theta\cos\varphi, r\sin\theta\sin\varphi, r\cos\theta) = {} & 2\sum_{\ell=0}^{\infty}\frac{1}{2\ell+1}\overline{P}_{\ell 0}(\cos\theta)\overline{P}_{\ell 0}(0)\frac{r_<^\ell}{r_>^{\ell+1}} \\ & - 4\Omega\sum_{\ell=1}^{\infty}\sum_{m=1}^{\ell} m\overline{P}_{\ell m}(\cos\theta)\overline{P}_{\ell m}(0) j_\ell(m\Omega r_<)[n_\ell(m\Omega r_>)\cos(m\varphi) + j_\ell(m\Omega r_>)\sin(m\varphi)].\end{aligned} \tag{A.4}$$

Here $\overline{P}_{\ell m}(u)$ is a normalized associated Legendre function, $j_\ell(z)$ and $n_\ell(z)$ are respectively spherical Bessel functions of the first and second kind [35], and $r_{>,<} = \max,\min(a,r)$. The series converges poorly near $r = a$, but converges rapidly for $r \gg a$ when $a\Omega \ll 1$.

To derive a different representation of the same solution which is valid near $r = a$, we take the retarded-time Liénard–Wiechert solution to (A.1), (cf. pages 280–282 of Ref. [42])

$$\Psi(t,\mathbf{x}) = \frac{1}{|\mathbf{x} - \boldsymbol{\xi}(t')| - \langle\dot{\boldsymbol{\xi}}(t'), \mathbf{x} - \boldsymbol{\xi}(t')\rangle} \tag{A.5}$$

and then evaluate it at a rotating observation point

$$\mathbf{x}(t) = z\mathbf{e}_z + \rho\cos(\varphi + \Omega t)\mathbf{e}_x + \rho\sin(\varphi + \Omega t)\mathbf{e}_y, \tag{A.6}$$

where $\rho^2 = x^2 + y^2 = \tilde{x}^2 + \tilde{y}^2$ and where φ is fixed. The evaluation point $\mathbf{x}(t)$ rotates with the source; whence this latter evaluation will effectively remove the time dependence from Ψ. In Eq. (A.5) $\langle,\rangle$ is the Euclidean inner product, $\dot{\boldsymbol{\xi}}(t')$ is the derivative of $\boldsymbol{\xi}(t')$ with respect to its argument, and the retarded time t' is the solution to

$$t - t' = |\mathbf{x} - \boldsymbol{\xi}(t')| = \left[z^2 + \rho^2 + a^2 - 2a\rho\cos(\phi - \Omega t')\right]^{1/2}. \tag{A.7}$$

Setting $\mathbf{x} = \mathbf{x}(t)$ and defining $\lambda \equiv t - t'$, we express the last equation as

$$\lambda = g(\lambda; a, \Omega, \rho, \varphi, z) \equiv \left[z^2 + \rho^2 + a^2 - 2a\rho\cos(\varphi + \Omega\lambda)\right]^{1/2}. \tag{A.8}$$

Since $a\Omega < 1$, (A.8) has a unique solution and the fixed-point iteration $\lambda_{n+1} = g(\lambda_n; a, \Omega, \rho, \varphi, z)$ converges for all choices of $a, \Omega, \rho, \varphi, z$. Finally, since $\psi(\tilde{x},\tilde{y},z) = \Psi(t,\mathbf{x}(t))$, we then have

$$\psi(\rho\cos\varphi, \rho\sin\varphi, z) = \frac{1}{\lambda - \rho a\Omega\sin(\varphi + \Omega\lambda)}. \tag{A.9}$$

References

[1] E.A. Coutsias, T. Hagstrom, J.S. Hesthaven, D. Torres, Integration preconditioners for differential operators in spectral τ-methods, Houston Journal of Mathematics 21 (1996) (spec. issue).
[2] E.A. Coutsias, T. Hagstrom, D. Torres, An efficient spectral method for ordinary differential equations with rational function coefficients, Math. Comput. 65 (214) (1996) 611–635.
[3] J.S. Hesthaven, Integration preconditioning of pseudospectral operators. I. Basic linear operators, SIAM J. Numer. Anal. 35 (4) (1998) 1571–1593.
[4] D.J. Torres, E.A. Coutsias, Pseudospectral solution of the two-dimensional Navier–Stokes equations in a disk, SIAM J. Sci. Comput. 21 (1) (1999) 378–403.
[5] G. von Winckel, S. Krishna, E.A. Coutsias, Spectral element modeling of semiconductor heterostructures, Math. Comput. Model. 43 (5–6) (2006) 582–591.
[6] S.R. Lau, R.H. Price, Multidomain spectral method for the helically reduced wave equation, J. Comput. Phys. 227 (2) (2007) 1126–1161.
[7] F. Pretorius, Evolution of binary black–hole spacetimes, Phys. Rev. Lett. 95 (2005) 121101 (4 pages).
[8] M. Campanelli, C.O. Lousto, P. Marronetti, Y. Zlochower, Accurate evolutions of orbiting black-hole binaries without excision, Phys. Rev. Lett. 96 (2006) 111101 (4 pages).
[9] J.G. Baker, J. Centrella, D.-I. Choi, M. Koppitz, J. van Meter, Gravitational-wave extraction from an inspiraling configuration of merging black holes, Phys. Rev. Lett. 96 (2006) 111102 (4 pages).
[10] M. Campanelli, C.O. Lousto, Y. Zlochower, Spinning-black-hole binaries: the orbital hang-up, Phys. Rev. D 74 (2006) 041501(R) (5 pages).
[11] M.A. Scheel, H.P. Pfeiffer, L. Lindblom, L.E. Kidder, O. Rinne, S.A. Teukolsky, Solving Einstein's equations with dual coordinate frames, Phys. Rev. D 74 (2006) 104006 (13 pages).
[12] M. Campanelli, C.O. Lousto, Y. Zlochower, B. Krishnan, D. Merritt, Spin flips and precession in black-hole-binary mergers, Phys. Rev. D 75 (2007) 064030 (17 pages).
[13] M. Boyle, D.A. Brown, L.E. Kidder, A.H. Mroué, H.P. Pfeiffer, M.A. Scheel, G.B. Cook, S.A. Teukolsky, High-accuracy comparison of numerical relativity simulations with post-Newtonian expansions, Phys. Rev. D 76 (2007) 124038 (31 pages).
[14] B. Brügmann, J.A. González, M. Hannam, S. Husa, U. Sperhake, Calibration of moving puncture simulations, Phys. Rev. D 77 (2008) 024027 (25 pages).
[15] M. Campanelli, C.O. Lousto, Y. Zlochower, Close encounters of three black holes, Phys. Rev. D 77 (2008) 101501(R) (5 pages).
[16] J.G. Baker, W.D. Boggs, J. Centrella, B.J. Kelly, S.T. McWilliams, M.C. Miller, J.R. van Meter, Modeling kicks from the merger of generic black hole binaries, Astrophys. J. 682 (1) (2008) L29–L32.
[17] J.G. Baker, W.D. Boggs, J. Centrella, B.J. Kelly, S.T. McWilliams, J.R. van Meter, Mergers of nonspinning black-hole binaries: Gravitational radiation characteristics, Phys. Rev. D 78 (2008) 044046 (25 pages).
[18] L. Rezzolla, E.N. Dorband, C. Reisswig, P. Diener, D. Pollney, E. Schnetter, B. Szilágyi, Spin diagrams for equal-mass black hole binaries with aligned spins, Astrophys. J. 679 (2) (2008) 1422–1426.
[19] M. Campanelli, C.O. Lousto, H. Nakano, Y. Zlochower, Comparison of numerical and post-Newtonian waveforms for generic precessing black-hole binaries, Phys. Rev. D 79 (2009) 084010 (24 pages).
[20] B. Szilágyi, L. Lindblom, M.A. Scheel, Simulations of binary black hole mergers using spectral methods, Phys. Rev. D 80 (2009) 124010 (17 pages).
[21] J.A. González, U. Sperhake, B. Brügmann, Black-hole binary simulations: the mass ratio 10:1, Phys. Rev. D 79 (2009) 124006 (10 pages).
[22] C.O. Lousto, Y. Zlochower, Orbital evolution of extreme-mass-ratio black-hole binaries with numerical relativity, Phys. Rev. Lett. 106 (2011) 041101 (4 pages).
[23] G. Lovelace, M.A. Scheel, B. Szilágyi, Simulating merging binary black holes with nearly extremal spins, Phys. Rev. D 83 (2011) 024010 (5 pages).
[24] J. Centrella, J.G. Baker, B.J. Kelly, J.R. van Meter, Black-hole binaries, gravitational waves, and numerical relativity, Rev. Mod. Phys. 82 (2010) 3069–3119.
[25] Z. Andrade, C. Beetle, A. Blinov, B. Bromley, L.M. Burko, M. Cranor, R. Owen, R.H. Price, The Periodic standing-wave approximation: overview and three dimensional scalar models, Phys. Rev. D 70 (2004) 064001 (14 pages).
[26] B. Bromley, R. Owen, R.H. Price, Periodic standing-wave approximation: nonlinear scalar fields, adapted coordinates, and the eigenspectral method, Phys. Rev. D 71 (2005) 104017 (27 pages).
[27] C. Beetle, B. Bromley, R.H. Price, Periodic standing-wave approximation: eigenspectral computations for linear gravity and nonlinear toy models, Phys. Rev. D 74 (2006) 024013 (17 pages).
[28] C. Beetle, B. Bromley, R.H. Price, Periodic standing-wave approximation: post-Minkowski computations, Phys. Rev. D 76 (2007) 084016 (16 pages).
[29] N. Hernández, R.H. Price, Periodic standing-wave approximation: computations in full general relativity, Phys. Rev. D 79 (2009) 064008 (13 pages).
[30] H. Pfeiffer, Initial data for black hole evolutions, Ph.D. thesis, Cornell University, 2003. Available from: <arXiv:gr-qc/0510016v1>.
[31] H.P. Pfeiffer, L.E. Kidder, M.A. Scheel, S.A. Teukolsky, A multidomain spectral method for solving elliptic equations, Comput. Phys. Commun. 152 (3) (2003) 253–273.
[32] Spectral Einstein Code, <www.black-holes.org/SpEC.html>.
[33] V. Frayssé, L. Giraud, S. Gratton, J. Langou, A Set of GMRES Routines for Real and Complex Arithmetics on High Performance Computers, CERFACS Technical Report TR/PA/03/3, July 2007. Available at <http://www.cerfacs.fr/algor/>.
[34] G.H. Golub, C.F. Van Loan, Matrix Computations, John Hopkins University Press, Baltimore, 1996.
[35] M. Abramowitz, I. Stegun, Handbook of Mathematical Functions, Dover, New York, 1972.
[36] I.J. Thompson, A.R. Barnett, Coulomb and Bessel functions of complex arguments and order, J. Comput. Phys. 64 (2) (1986) 490–509.
[37] E.L. Hill, R. Landshoff, The Dirac electron theory, Rev. Mod. Phys. 10 (1938) 87–132.
[38] See <arXiv:1106.1632v1 [gr-qc]> for more details.
[39] B. Smith, P. Bjrstad, W. Gropp, Domain Decomposition: Parallel Multilevel Methods for Elliptic Partial Differential Equations, Cambridge University Press, Cambridge, UK, 1996.
[40] J.C. Adams, P.N. Swarztrauber, SPHEREPACK 3.0: a model development facility, Mon. Wea. Rev. 127 (1999) 1872–1878.
[41] G.A. Schott, Electromagnetic Radiation and the Mechanical Reactions Arising from it, Cambridge University Press, 1912.
[42] J. Mathews, R.L. Walker, Mathematical Methods of Physics, second edition., W.A. Benjamin, Inc., New York, 1970.
[43] J. Bičák, B.G. Schmidt, Helical symmetry in linear systems, Phys. Rev. D 76 (2007) 104040 (11 pages).